† Research sponsored by the U. S. Atomic Energy Commission under contract with Union Carbide Corporation.

[1]L. W. Chiao and M. J. Martin, Nucl. Data B2 (No. 1), 81 (1967).
[2]I. Adam, K. S. Toth, and M. F. Roche, Nucl. Phys. A121, 289 (1968).
[3]R. Gunnink, J. B. Niday, R. P. Anderson, and R. A. Meyer, Lawrence Livermore Laboratory Report No. UCID-15439, 1969 (unpublished).
[4]Y. Y. Chu, E. M. Franz, and G. Friedlander, Phys. Rev. 175, 1523 (1968).
[5]L. A. Sliv and I. M. Band, in *Alpha-, Beta-, and Gamma-Ray Spectroscopy,* edited by K. Siegbahn (North-Holland, Amsterdam, 1965), Appendix 5.
[6]I. Adam, K. Wilski, Zh. Zhelev, M. Jørgensen, M. Krivopustov, V. Kuznetsov, O. B. Nielsen, and M. Finger, Dubna Report No. P-2581, 1966 (unpublished).
[7]R. K. Jolly and C. F. Moore, Phys. Rev. 145, 918 (1966).
[8]P. R. Christensen, B. Herskind, R. R. Borchers, and L. Westgaard, Nucl. Phys. A102, 481 (1967).
[9]R. A. Kenefick and R. K. Sheline, Phys. Rev. 139, B1479 (1965).
[10]G. J. Nijgh, A. H. Wapstra, and R. Van Lieshout, *Nuclear Spectroscopy Tables* (North-Holland, Amsterdam, 1959), Chap. 5, Sec. 4, pp. 58–65.
[11]E. Newman, K. S. Toth, R. L. Auble, R. M. Gaedke, M. F. Roche, and B. H. Wildenthal, Phys. Rev. C 1, 1118 (1970).
[12]R. H. Fulmer, A. L. McCarthy, and B. L. Cohen, Phys. Rev. 128, 1302 (1962).
[13]C. A. Wiedner, A. Heusler, J. Solf, and J. B. Wurm, Nucl. Phys. A103, 433 (1967).
[14]L. Veeser and W. Haeberli, Nucl. Phys. A115, 172 (1968).
[15]P. A. Moore, P. J. Riley, C. M. Jones, M. D. Mancusi, and J. L. Foster, Jr., Phys. Rev. 175, 1516 (1968).
[16]D. von Ehrenstein, G. C. Morrison, J. A. Nolen, Jr., and N. Williams, Phys. Rev. C 1, 2066 (1970).
[17]M. P. Avotina and A. V. Zolotavin, *Isobaric Nuclei With Mass Number A = 147,* issue No. 11 of Properties of Atomic Nuclei (Publishing House "Science," Leningrad Section, Leningrad, 1971).

PHYSICAL REVIEW C VOLUME 7, NUMBER 1 JANUARY 1973

Hartree-Fock Calculations with Skyrme's Interaction. II. Axially Deformed Nuclei*

D. Vautherin
Laboratory for Nuclear Science and Department of Physics, Massachusetts Institute of Technology, Cambridge, Massachusetts 02139,
and Institut de Physique Nucléaire, Division de Physique Théorique, Laboratoire Associé au Centre National de la Recherche Scientifique 91 Orsay, France
(Received 31 July 1972)

Skyrme's interaction is used in deformed Hartree-Fock calculations of some light and rare-earth nuclei. A method of solution is presented, which exploits as much as possible the simple features of the Skyrme force in order to allow calculations of heavy deformed nuclei. In the rare-earth region pairing correlations are taken into account in a simplified but self-consistent way by considering energy functionals depending also on occupation probabilities. Calculations have been made for the two parameter sets which were used in a previous study of double-closed-shell nuclei. The set providing the best fit to ground-state properties of spherical nuclei is also found to give a satisfactory description of nuclear deformations. Comparison is made with other available Hartree-Fock calculations in the case of light nuclei, and a discussion of the importance of various terms in the effective force upon nuclear deformations is given.

I. INTRODUCTION

Skyrme's interaction[1] has been shown in a previous paper[2] to give a very good description of ground-state properties of spherical nuclei in the Hartree-Fock approximation. In particular remarkable fits to binding energies, radii, and elastic electron scattering cross sections have been obtained. Also, single-particle level densities near the Fermi level were found to be reasonably close to the observed ones. Such an agreement has been shown to be related to the density dependence of the Skyrme force. Similar results were indeed obtained from other density-dependent effective forces[3,4] and from realistic Brueckner-Hartree-Fock calculations in the local density approximation.[5,6]

The purpose of this paper is to extend our previous investigations to deformed nuclei. As compared to earlier studies of nuclear deformations in the framework of the Hartree-Fock theory, the present calculations will be shown to achieve at

least one significant improvement. Indeed, while available Hartree-Fock calculations of deformed nuclei have been restricted to light nuclei,[7-15] we will see that, thanks to its computational simplicity, the Skyrme force allows studies of nuclear deformations in the rare-earth region, where the validity of the rotational model is best established.

From the Nilsson model,[16] equilibrium shapes of nuclei are known to be extremely sensitive to level spacings. Since single-particle spectra obtained from the Skyrme force are among the closest to the experimental ones in Hartree-Fock calculations, one may hope that this interaction, which was adjusted to properties of some doubly-closed-shell nuclei, will also give a reasonable description of nuclear deformations. In such case, the use of the Skyrme force in Hartree-Fock calculations would provide a powerful and rather reliable tool to extrapolate to properties of nuclei far off the stability line and to superheavy nuclei.

Let us also recall that the parameters of Skyrme's interaction may be related to realistic reaction matrices by means of an expansion for the density matrix.[17] Calculations of the present type may therefore appear as a first step towards a description of deformations in the region of heavy nuclei based on a realistic nucleon-nucleon force.

In Sec. II a summary of the basic equations to be solved is given, and an outline of the method of solution is presented in the most general case of nonaxial deformations. To take advantage of the simplicity of the Hartree-Fock equations for Skyrme's interaction this method uses two different representations during the iteration procedure. The average field is evaluated from the wave functions in coordinate space while the solution of the deformed Schrödinger equation is carried out in an oscillator basis. In the case of even-even nuclei the Hartree-Fock equations have solutions with axial symmetry, which results in the elimination of the azimuthal variable. This reduction is made in Sec. III where some invariance properties of the Hartree-Fock equations are also discussed. The particular type of nonlocality of the average field encountered for Skyrme's interaction allows a solution of the deformed Schrödinger equation by a straightforward extension of the method of Damgaard *et al.*[18] An outline of this method is given in Sec. IV where its extension to the present case of a radius-dependent effective mass is also described. In Sec. V a reconstruction of densities in the coordinate space from the oscillator expansion coefficients is made since the evaluation of the Hartree-Fock field is most easily carried out in this representation. In Sec. VI a formula suitable for a numerical calculation of the Coulomb potential in configuration space is derived, while the problem of pairing effects is treated in Sec. VII. These effects are included by considering energy functionals which depend on occupation probabilities. General properties of such functionals are investigated and it is shown in particular that any given occupation-probability distribution may be derived from a variational principle. The solution of this problem is found to depend on an arbitrary function. This degree of freedom is used to construct the simplest possible set of equations, namely a set of Hartree-Fock plus BCS equations[19] with a constant gap.

Results for some light and rare-earth nuclei, obtained from the two different forces already used in Ref. 2, are presented and discussed in Sec. VIII. In the case of light nuclei, comparison is made with results of other Hartree-Fock calculations. The convergence of the oscillator expansion is also discussed and the influence of various terms in the effective force upon nuclear deformations is investigated.

II. HARTREE-FOCK EQUATIONS

The system of Hartree-Fock equations for the Skyrme interaction was derived in Ref. 2 assuming time-reversal invariance only. Since no assumption was made concerning the shape of the system, this set of equations is also valid in the case of a deformed nucleus. Neglecting the small contribution of the central force to the one-body spin-orbit potential, as was justified in Ref. 2, the Hartree-Fock equations for the single-particle wave functions $\Phi_i(\vec{R}, \sigma, q)$, where $\vec{R}$, σ, and q denote the space, spin, and isospin coordinates of one nucleon, respectively, may be written as

$$\left[-\vec{\nabla}\cdot\frac{\hbar^2}{2m^*(\vec{R})}\vec{\nabla}+U(\vec{R})+\vec{\nabla}W(R)\cdot(-i)(\vec{\nabla}\times\vec{\sigma})\right]\Phi_i=e_i\Phi_i\,. \tag{2.1}$$

In Eq. (2.1) the effective mass and the central- and spin-orbit potentials in the case of a neutron state are given by

$$\begin{aligned}U_n(\vec{R})=t_0[(1+\tfrac{1}{2}x_0)\rho-(x_0+\tfrac{1}{2})\rho_n]+\tfrac{1}{4}t_3\rho_p(\rho+\rho_n)\\ -\tfrac{1}{8}(3t_1-t_2)\nabla^2\rho+\tfrac{1}{16}(3t_1+t_2)\nabla^2\rho_n\\ +\tfrac{1}{4}(t_1+t_2)\tau+\tfrac{1}{8}(t_2-t_1)\tau_n-\tfrac{1}{2}W_0(\mathrm{div}\vec{J}+\mathrm{div}\vec{J}_n)\,,\end{aligned} \tag{2.2a}$$

$$\frac{\hbar^2}{2m_n^*(\vec{R})}=\frac{\hbar^2}{2m}+\tfrac{1}{4}(t_1+t_2)\rho+\tfrac{1}{8}(t_2-t_1)\rho_n\,, \tag{2.2b}$$

$$W_n(\vec{R})=\tfrac{1}{2}W_0(\rho+\rho_n)\,. \tag{2.2c}$$

The corresponding equations for a proton state are obtained by interchanging the indices n and p in Eqs. (2.2), and by adding to the central field (2.2a) the Coulomb field

$$V_C(\vec{R}) = e^2 \int d^3\vec{R}' \frac{\rho_p(\vec{R}')}{|\vec{R}-\vec{R}'|} . \tag{2.3}$$

As in the calculations we made in Ref. 2 for spherical nuclei, the Coulomb exchange term has been neglected. The nucleon densities $\rho_n(\vec{R})$, $\rho_p(\vec{R})$; the kinetic energy densities $\tau_n(\vec{R})$, $\tau_p(\vec{R})$; and the spin densities $\vec{J}_n(\vec{R})$, $\vec{J}_p(\vec{R})$ appearing in Eqs. (2.2) were defined in Ref. 2, and the constants t_0, t_1, t_2, t_3, x_0, W_0 are the parameters of the Skyrme force. In Ref. 2 we constructed two different sets of parameters denoted by I and II, which are listed for completeness in Table I. These were shown to give similar results for binding energies and radii of spherical nuclei, but rather different predictions concerning $1s$-proton levels due to different values of the effective mass m^*/m in nuclear matter, i.e., as may be seen from Eq. (2.1), different nonlocalities in the average nuclear field.

For spherical nuclei the previous set of equations was solved through the usual iteration procedure which contains two distinct steps. A first one is to solve the Schrödinger equation corresponding to given values of the effective mass $\hbar^2/2m^*$, of the potential U and of the one-body spin-orbit potential W. The second step consists in evaluating these quantities from the wave functions Φ_i. This whole procedure was carried out in coordinate space in Ref. 2, since it is the most convenient representation to exploit the simplicity of the algebraic relations (2.2) between the potential and the densities. Also, the Schrödinger equation (2.1) reduces in this latter case to a radial differential equation. In the case of deformed nuclei, however, the situation is more complicated since solving a deformed Schrödinger equation in coordinate space is a difficult problem.[20] On the other hand, the evaluation of the average field from Eqs. (2.2) is most efficiently carried out in this representation, whereas the use of an oscillator basis would introduce severe limitations associated with storage of matrix elements and computation time. For these reasons, the method we have constructed uses two different representations for the two previous steps of the iteration procedure. The solution of the deformed Schrödinger equation has been carried out in a deformed oscillator basis, while the evaluation of the potential has been made in coordinate space. As an additional step our method therefore includes a reconstruction of the densities in coordinate space from the wave functions obtained in the oscillator basis. Such a method is applicable to nonaxial deformations. However, in this present work it will be applied to axially symmetric shapes only. Furthermore, we will consider only reflection symmetric shapes.

TABLE I. Numerical values of the parameters t_0 (MeV fm^3), t_1 (MeV fm^5), t_2 (MeV fm^5), t_3 (MeV fm^6), W_0 (MeV fm^5), and x_0 corresponding to interactions I and II of Ref. 2. The value of the effective mass m^*/m in infinite nuclear matter is also given.

	t_0	t_1	t_2	t_3	x_0	W_0	m^*/m
I	−1057.3	235.9	−100	14463.5	0.56	120	0.911
II	−1169.9	585.6	−27.1	9331.1	0.34	105	0.580

III. CASE OF AXIALLY DEFORMED NUCLEI

In the case of even-even nuclei considered here the Hartree-Fock equations (2.1, 2.2) have solutions with axial symmetry. Assuming the symmetry axis to be the z axis, this means that the third component J_z of the total angular momentum is a good quantum number for the single-particle state Φ_i. In other words if we denote by Ω_i the eigenvalue of J_z associated with the single-particle state i, there are solutions of the form

$$\Phi_i(\vec{R}, \sigma, q) = \chi_{q_i}(q)[\Phi_i^+(r, z)e^{i\Lambda^- \varphi}\chi_{+1/2}(\sigma) + \Phi_i^-(r, z)e^{i\Lambda^+\varphi}\chi_{-1/2}(\sigma)], \tag{3.1}$$

where

$$\Lambda^{\pm} = \Omega_i \pm \tfrac{1}{2} . \tag{3.2}$$

In Eq. (3.1) the quantities r, z, and φ are the cylindrical coordinates of $\vec{R}$:

$$R_x = r\cos\varphi , \quad R_y = r\sin\varphi , \quad R_z = z . \tag{3.3}$$

We have also assumed the Hartree-Fock states i to be eigenstates of the third component τ_z of the isospin operator with a corresponding eigenvalue $q_i = +\frac{1}{2}$ for protons, $-\frac{1}{2}$ for neutrons. For such nuclei the system of Hartree-Fock equations can be reduced to a system involving the variables r and z only by substituting the ansatz (3.1) into Eqs. (2.1) and (2.2). From the definitions given in Ref. 2 for the nucleon and kinetic energy densities one first obtains that these functions depend on the coordinates r and z only. Explicitly:

$$\rho(r, z) = \sum_i [|\Phi_i^+(r, z)|^2 + |\Phi_i^-(r, z)|^2] , \tag{3.4a}$$

$$\tau(r,z)=\sum_i\Big(|\nabla_r\Phi_i^+(r,z)|^2+|\nabla_z\Phi_i^+(r,z)|^2 +\frac{1}{r^2}|\Lambda^-\Phi_i^+(r,z)|^2+|\nabla_r\Phi_i^-(r,z)|^2 +|\nabla_z\Phi_i^-(r,z)|^2+\frac{1}{r^2}|\Lambda^+\Phi_i^-(r,z)|^2\Big). \tag{3.4b}$$

In Eqs. (3.4) the sums run over neutron (proton) states to obtain neutron (proton) densities. We have used the components of the gradient operator in cylindrical coordinates

$$\nabla_r=\frac{\partial}{\partial r},\quad \nabla_z=\frac{\partial}{\partial z},\quad \nabla_\varphi=\frac{1}{r}\frac{\partial}{\partial\varphi}=\frac{i\hat{l}_z}{r}, \tag{3.5}$$

to derive the expression for $\tau(r,z)$. As will be seen later, time-reversal invariance allows further simplifications of Eqs. (3.4). From the definition given in Ref. 2 for the spin density $\vec{J}$, one has the following expression for $\mathrm{div}\vec{J}$:

$$\mathrm{div}\vec{J}=(-i)\sum_{i\sigma q}\vec{\nabla}\Phi_i^*(\vec{R},\sigma,q)\cdot(\vec{\nabla}\times\vec{\sigma})\Phi_i(\vec{R},\sigma,q). \tag{3.6}$$

Writing the components of the operator $\vec{\nabla}\times\vec{\sigma}$ as

$$(-i)(\vec{\nabla}\times\vec{\sigma})_r=\sigma_z\frac{\hat{l}_z}{r}+\tfrac{1}{2}(\sigma_+e^{-i\varphi}-\sigma_-e^{+i\varphi})\nabla_z,$$

$$(-i)(\vec{\nabla}\times\vec{\sigma})_z=-\tfrac{1}{2}\sigma_+e^{-i\varphi}\Big(\nabla_r+\frac{\hat{l}_z}{r}\Big)+\tfrac{1}{2}\sigma_-e^{i\varphi}\Big(\nabla_r-\frac{\hat{l}_z}{r}\Big),$$

$$(\vec{\nabla}\times\vec{\sigma})_\varphi=\tfrac{1}{2}(\sigma_+e^{-i\varphi}+\sigma_-e^{i\varphi})\nabla_z-\sigma_z\nabla_r, \tag{3.7}$$

and using the components (3.5) for the gradient operator in cylindrical coordinates, expression (3.6) reduces to

$$\mathrm{div}\vec{J}(r,z)=2\sum_i\Big(\nabla_r\Phi_i^+(r,z)\nabla_z\Phi_i^-(r,z)-\nabla_r\Phi_i^-(r,z)\nabla_z\Phi_i^+(r,z) +\frac{\Lambda^-}{r}\Phi_i^+(r,z)[\nabla_r\Phi_i^+(r,z)-\nabla_z\Phi_i^-(r,z)]-\frac{\Lambda^+}{r}\Phi_i^-(r,z)[\nabla_z\Phi_i^+(r,z)+\nabla_r\Phi_i^-(r,z)]\Big). \tag{3.8}$$

Since densities depend on the coordinates r and z only, the same will hold for the effective mass and for the central and spin-orbit potentials due to Eq. (2.2). Then inserting expressions (3.1) into Eq. (2.1) one obtains, by means of Eq. (3.7), the following set of coupled equations for the components $\Phi_i^+(r,z)$ and $\Phi_i^-(r,z)$:

$$-\nabla_r\Big\{\frac{\hbar^2}{2m_q^*}\nabla_r\Phi_i^+\Big\}-\nabla_z\Big\{\frac{\hbar^2}{2m_q^*}\nabla_z\Phi_i^+\Big\}+\frac{1}{r^2}(\Lambda^-)^2\Phi_i^++U_q(r,z)\Phi_i^+ +\nabla_rW_q(r,z)\Big(\nabla_z\Phi_i^-+\frac{\Lambda^-}{r}\Phi_i^+\Big)-\nabla_zW_q(r,z)\Big(\nabla_r\Phi_i^-+\frac{\Lambda^+}{r}\Phi_i^-\Big)=e_i\Phi_i^+,$$

$$-\nabla_r\Big\{\frac{\hbar^2}{2m_q^*}\nabla_r\Phi_i^-\Big\}-\nabla_z\Big\{\frac{\hbar^2}{2m_q^*}\nabla_z\Phi_i^-\Big\}+\frac{1}{r^2}(\Lambda^+)^2\Phi_i^-+U_q(r,z)\Phi_i^- -\nabla_rW_q(r,z)\Big(\nabla_z\Phi_i^++\frac{\Lambda^+}{r}\Phi_i^-\Big)+\nabla_zW_q(r,z)\Big(\nabla_r\Phi_i^+-\frac{\Lambda^-}{r}\Phi_i^+\Big)=e_i\Phi_i^-, \tag{3.9}$$

where q stands for the charge of the single-particle state i. This step achieves the reduction of the Hartree-Fock equations in cylindrical coordinates.

From Eqs. (3.9) one may easily observe that, if a state Φ_i [defined from expression (3.1) by a set $\{\Phi^+,\Phi^-,\Omega\}$] satisfies the Schrödinger equation (2.1), then the state

$$\Phi_{\bar{i}}=\{-\Phi^-,\Phi^+,-\Omega\} \tag{3.10}$$

also satisfies Eq. (2.1) with the same eigenvalue e_i. This property is just a consequence of time-reversal invariance. Indeed applying to Φ_i the time-reversal operator

$$K=-i\sigma_yK_0=\tfrac{1}{2}(\sigma_--\sigma_+)K_0, \tag{3.11}$$

where K_0 denotes the complex conjugation operator in configuration space, one concludes immediately that $\bar{i}$ is the time-reversed state associated with i.

Contributions of time-reversed states i and $\bar{i}$ to the densities (3.4) and (3.8) may be seen to be identical. Since we assume the set of occupied states to be invariant under time reversal, we can use the previous symmetry property to restrict the sums in Eqs. (3.4) and (3.8) to positive values of

Ω_i, provided the total results are multiplied by a factor 2.

A similar discussion can be made concerning parity. If the single-particle states (3.1) are assumed to be eigenstates of the parity operator one can see that the densities (3.4) and (3.8) are reflection symmetric so that the same property holds for the effective mass and for central and spin-orbit potentials. In such a case only positive values of z need to be considered in the previous equations.

IV. SOLUTION OF THE DEFORMED SCHRÖDINGER EQUATION

A. Definitions and Notations

The solution of the deformed Schrödinger equation with an effective mass (2.1) may be obtained by a straightforward extension of the method worked out by Damgaard *et al.*[18] in the case of a local potential. In this method the unknown wave functions Φ_i are expended into eigenfunctions of an axially deformed harmonic-oscillator potential

$$V(r, z) = \tfrac{1}{2} m \omega_\perp{}^2 r^2 + \tfrac{1}{2} m \omega_z{}^2 z^2 . \tag{4.1}$$

Introducing the oscillator constants

$$\beta_z = \frac{1}{b_z} = (m\omega_z/\hbar)^{1/2}, \quad \beta_\perp = \frac{1}{b_\perp} = (m\omega_\perp/\hbar)^{1/2}, \tag{4.2}$$

and the auxiliary variables

$$\xi = z\beta_z, \quad \eta = r^2 \beta_\perp{}^2 , \tag{4.3}$$

these eigenfunctions may be written explicitly as

$$\varphi_{n_r n_z \Lambda\Sigma}(\vec{\mathrm{R}}, \sigma) = \psi^\Lambda_{n_r}(r)\psi_{n_z}(z)\frac{e^{i\Lambda\varphi}}{\sqrt{2\pi}}\chi_\Sigma(\sigma), \tag{4.4}$$

where

$$\psi_{n_z}(z) = N_{n_z}\beta_z{}^{1/2} e^{-\xi^2/2} H_{n_z}(\xi), \tag{4.5a}$$

$$\psi^\Lambda_{n_r}(r) = N^\Lambda_{n_r}\beta_\perp \sqrt{2}\,\eta^{\Lambda/2} e^{-\eta/2} L^\Lambda_{n_r}(\eta). \tag{4.5b}$$

In Eqs. (4.5), $H_{n_z}(\xi)$ and $L^\Lambda_{n_r}(\eta)$ denote Hermite and associated Laguerre polynomials,[21] and the corresponding normalization factors are

$$N_{n_z} = \left(\frac{1}{\sqrt{\pi}\, 2^{n_z} n_z!}\right)^{1/2}, \quad N^\Lambda_{n_r} = \left(\frac{n_r!}{(n_r+\Lambda)!}\right)^{1/2}. \tag{4.6}$$

From these expressions, the quantum numbers appearing in Eq. (4.4) may be interpreted as follows: n_r and n_z are the number of nodes in the r and z directions, respectively, and Λ and Σ are the projections on the z axis of orbital angular momentum and spin, respectively. For simplicity a single index α will be used to denote the previous set of quantum numbers

$$\alpha \equiv \{n_r, n_z, \Lambda, \Sigma\}. \tag{4.7}$$

The eigenvalue associated with such a state is

$$E_\alpha = (2n_r + |\Lambda| + 1)\hbar\omega_\perp + (n_z + \tfrac{1}{2})\hbar\omega_z . \tag{4.8}$$

For notational convenience we also define polynomials $\tilde{H}_{n_z}$ and $\tilde{L}^\Lambda_{n_r}$, which will be needed in the evaluation of matrix elements, by the following relations:

$$\nabla_z \psi_{n_z}(z) = N_{n_z}\beta_z{}^{3/2} e^{-\xi^2/2}\tilde{H}_{n_z}(\xi), \tag{4.9a}$$

$$\nabla_r \psi^\Lambda_{n_r}(r) = N^\Lambda_{n_r}\beta_\perp{}^2\sqrt{2}\,\eta^{(\Lambda-1)/2}\tilde{L}^\Lambda_{n_r}(\eta). \tag{4.9b}$$

Using the expressions for the derivatives of the Hermite and associated Laguerre polynomials and their recursion formulas,[21] one finds that

$$\tilde{H}_{n_z}(\xi) = \xi H_{n_z}(\xi) - H_{n_z+1}(\xi), \tag{4.10a}$$

$$\tilde{L}^\Lambda_{n_r}(\eta) = 2(n_r+1)L^\Lambda_{n_r+1}(\eta) - (2n_r + \Lambda + 2 - \eta)L^\Lambda_{n_r}(\eta). \tag{4.10b}$$

Since we assume our Hartree-Fock states to be eigenstates of the charge operator, the expansion of the single-particle Hartree-Fock orbitals is of the form

$$\Phi_i(\vec{\mathrm{R}}, \sigma, q) = \chi_{q_i}(q)\sum_\alpha C^i_\alpha \varphi_\alpha(\vec{\mathrm{R}}, \sigma), \tag{4.11}$$

where q_i denotes the charge of the state i. Inserting expression (4.11) into the Schrödinger equation (2.1) and using the orthogonality of the basis states we find that the expansion coefficients have to be eigenvectors of the Hamiltonian matrix

$$\sum_\beta H^{(q_i)}_{\alpha\beta} C^i_\beta = e_i C^i_\alpha, \tag{4.12}$$

where

$$H^{(q)}_{\alpha\beta} = \left\langle \alpha \left| -\vec{\nabla}\cdot\frac{\hbar^2}{2m^*_q}\vec{\nabla} + U_q + \vec{\nabla}W_q \cdot (-i)(\vec{\nabla}\times\vec{\sigma}) \right| \beta \right\rangle . \tag{4.13}$$

Now, in the case of axially deformed nuclei we are interested in, the third component of the total angular momentum $\Omega = \Lambda + \Sigma$ is a good quantum number and therefore, $H_{\alpha\beta}$ is block diagonal, each block being characterized by Ω. Furthermore, since we consider only reflection symmetric shapes, the parity $\pi = (-1)^{n_z+\Lambda}$ is also a good quantum number and each of the previous blocks then falls into two submatrices characterized by values of Ω and π. Finally, due to the time-reversal symmetry property (3.10) the Hamiltonian matrix needs to be constructed for positive values of Ω only.

The standard way of solving the infinite dimensional problem (4.12) is to use a truncated basis, i.e., to restrict the sum over α in (4.11) to a sum of N terms, this number N being in principle ultimately increased until convergence for the expansion coefficients is reached. In our calculations this procedure has been carried out by including in (4.11) all states for which the total number of quanta in the xy plane and the z direction is less than or equal to a certain fixed number N_0, i.e.,

$$2n_r + n_z + \Lambda \leq N_0 . \tag{4.14}$$

As shown in Appendix A the number of such states corresponding to a positive value of Ω is given by

$$N = \tfrac{1}{6}(N_0+1)(N_0+2)(N_0+3) . \tag{4.15}$$

In this basis the Hamiltonian matrix (4.13) splits up into $2N_0+1$ submatrices associated with positive values of Ω and $2N_0+1$ submatrices associated with negative values of Ω. The largest blocks correspond to $\Omega = \pm\frac{1}{2}$, $\pi = +1$ and have a dimension of $(N_0+2)^2/4$ (N_0 even). For storage purposes and evaluation of computation times in numerical applications, it is also convenient to know the number $F(N_0)$ of nonvanishing matrix elements in $H_{\alpha\beta}$ corresponding to $\Omega > 0$. This number is shown in Appendix A to be

$$F(N_0) = \tfrac{1}{40}(N_0+2)(N_0^2+2N_0+2)(N_0^2+6N_0+10) . \tag{4.16}$$

In order to allow investigations of truncation effects, the code we have constructed can include a total number of 15 major shells, i.e., $N_0 \leq 14$. However, since computation times increase quite rapidly with N_0, calculations have been restricted to $N_0 \leq 8$.

B. Choice of the Oscillator Parameters

Truncation effects in the case of an expansion into the basis vectors (4.4) depend on the shape of the nucleus: As was noted by Damgaard *et al.*,[18] the mixing of the basis states is largest for spherical nuclei, while for deformed nuclei, expansion (4.11) may involve only a few relevant components. The previous effects also depend critically upon the choice of the oscillator parameters and it was shown by Tuerpe, Bassichis, and Kerman[7] that it is rather crucial to minimize the total energy with respect to both oscillator parameters β_z and $\beta_\perp$. In particular these authors find that their results in iron-52 with a $N_0 = 6$ spherical basis may be reproduced in a $N_0 = 4$ deformed basis alone with parameters chosen by minimizing total energy with respect to β_z and $\beta_\perp$. For this reason, in all calculations presented here, this minimization procedure has been carried out.

Such a procedure may be performed in a very simple way for the volume parameter

$$\beta_0 = (m\omega_0/\hbar)^{1/2} , \quad \omega_0 = (\omega_\perp{}^2\omega_z)^{1/3} . \tag{4.17}$$

Indeed, for given values of the expansion coefficients in Eq. (4.11), it may be readily seen from Eqs. (10) and (12) of Ref. 2 that the total energy is a polynomial of sixth degree in β_0, whose coefficients may be readily evaluated. Therefore, at the end of each iteration in the numerical solution, the value of β_0 may be readjusted so as to simultaneously minimize with respect to the volume oscillator parameter.

In the case of the deformation parameter

$$q = \omega_\perp/\omega_z = \beta_\perp{}^2/\beta_z{}^2 , \tag{4.18}$$

the previous minimization procedure has been carried out numerically, using a 0.1-step and a three-point interpolation formula in the neighborhood of the minimum.

C. Calculation of Matrix Elements

The solution of the Schrödinger equation involves as an intermediate step a calculation of the matrix elements (4.13) from the effective mass $\hbar^2/2m^*(r,z)$ and from the central and spin-orbit potentials $U(r,z)$ and $W(r,z)$, respectively. Integrating by parts, the matrix element for the kinetic energy term becomes

$$\left\langle \alpha \left| -\vec{\nabla}\cdot\frac{\hbar^2}{2m^*(r,z)}\vec{\nabla} \right| \beta \right\rangle = \sum_\sigma \int d^3R \, \frac{\hbar^2}{2m^*(r,z)} \vec{\nabla}\varphi_\alpha^*(R,\sigma)\cdot\vec{\nabla}\varphi_\beta(\vec{R},\sigma) . \tag{4.19}$$

Using the components (3.5) of the gradient operator in cylindrical coordinates, the right-hand side of Eq. (4.19) may be written as

$$\delta_{\Lambda\Lambda'}\delta_{\Sigma\Sigma'} \int_0^{+\infty} r\,dr \int_{-\infty}^{+\infty} dz \frac{\hbar^2}{2m^*(r,z)} \Big(\nabla_z\psi_{n_z}(z)\nabla_z\psi_{n_z'}(z)\psi_{n_r}^{\Lambda}(r)\psi_{n_r'}^{\Lambda'}(r) + \psi_{n_z}(z)\psi_{n_z'}(z)\nabla_r\psi_{n_r}^{\Lambda}(r)\nabla_r\psi_{n_r'}^{\Lambda'}(r) + \frac{\Lambda\Lambda'}{r^2}\psi_{n_z}(z)\psi_{n_z'}(z)\psi_{n_r}^{\Lambda}(r)\psi_{n_r'}^{\Lambda'}(r) \Big) . \tag{4.20}$$

In Eq. (4.20) the quantum numbers $\alpha \equiv n_r n_z \Lambda \Sigma$ and $\beta \equiv n_r' n_z' \Lambda' \Sigma'$ have been written explicitly. Finally using the definitions (4.5) and (4.9) one obtains the following expression:

$$\delta_{\Lambda\Lambda'}\delta_{\Sigma\Sigma'}N_{n_z}N_{n_z'}N^{\Lambda}_{n_r}N^{\Lambda'}_{n_r'}\int_0^{+\infty}d\eta\,\eta^{\Lambda-1}e^{-\eta}\int_{-\infty}^{+\infty}e^{-\xi^2}d\xi$$
$$\times\ \{\beta_z^2\tilde{H}_{n_z}(\xi)\tilde{H}_{n_z'}(\xi)L^{\Lambda}_{n_r}(\eta)L^{\Lambda'}_{n_r'}(\eta)\times\eta+\beta_\perp{}^2H_{n_z}(\xi)H_{n_z'}(\xi)[\tilde{L}^{\Lambda}_{n_r}(\eta)\tilde{L}^{\Lambda'}_{n_r'}(\eta)+\Lambda\Lambda' L^{\Lambda}_{n_r}(\eta)L^{\Lambda'}_{n_r'}(\eta)]\}\frac{\hbar^2}{2m^*(b_\perp\eta^{1/2},\,b_z\xi)}, \tag{4.21}$$

where b_z and $b_\perp$ are defined by Eq. (4.2).

Since the matrix elements for a central and for a spin-orbit potential have been evaluated by Damgaard *et al.*[18] this calculation will not be repeated here and we will just give the final expressions using our notations for completeness. For a central potential it is found that the matrix elements are given by

$$\langle\alpha|U|\beta\rangle=\delta_{\Lambda\Lambda'}\delta_{\Sigma\Sigma'}N_{n_z}N_{n_z'}N^{\Lambda}_{n_r}N^{\Lambda'}_{n_r'}\int_0^{+\infty}d\eta\,\eta^{\Lambda}e^{-\eta}\int_{-\infty}^{+\infty}e^{-\xi^2}d\xi\,H_{n_z}(\xi)H_{n_z'}(\xi)L^{\Lambda}_{n_r}(\eta)L^{\Lambda'}_{n_r'}(\eta)U(b_\perp\eta^{1/2},\,b_z\xi)\,. \tag{4.22}$$

For a spin-orbit potential the corresponding expression is a little more complicated since such a potential mixes states with different values of Σ. The result, which can be obtained from Eqs. (3.9) is

$$\langle\alpha|-i\vec{\nabla}W(r,z)\cdot(\vec{\nabla}\times\vec{\sigma})|\beta\rangle=N_{n_z}N_{n_z'}N^{\Lambda}_{n_r}N^{\Lambda'}_{n_r'}\int_{-\infty}^{+\infty}e^{-\xi^2}d\xi\int_0^{+\infty}e^{-\eta}\eta^{(\Lambda+\Lambda'-2)/2}d\eta$$
$$\times\Big(-2\delta_{\Sigma\Sigma'}\delta_{\Lambda\Lambda'}\Sigma\Lambda\beta_\perp{}^2H_{n_z}(\xi)H_{n_z'}(\xi)[\tilde{L}^{\Lambda}_{n_r}(\eta)L^{\Lambda'}_{n_r'}(\eta)+L^{\Lambda}_{n_r}(\eta)\tilde{L}^{\Lambda'}_{n_r'}(\eta)]$$
$$+(1-\delta_{\Sigma\Sigma'})\beta_z\beta_\perp\eta^{1/2}\{\tilde{H}_{n_z}(\xi)H_{n_z'}(\xi)L^{\Lambda}_{n_r}(\eta)[(\Lambda'-\Lambda)\tilde{L}^{\Lambda'}_{n_r'}(\eta)+\Lambda' L^{\Lambda'}_{n_r'}(\eta)]$$
$$+\tilde{H}_{n_z'}(\xi)H_{n_z}(\xi)L^{\Lambda'}_{n_r'}(\eta)[(\Lambda-\Lambda')\tilde{L}^{\Lambda}_{n_r}(\eta)+\Lambda L^{\Lambda}_{n_r}(\eta)]\}\Big)W(b_\perp\eta^{1/2},\,b_z\xi)\,. \tag{4.23}$$

In practice the integrations in Eqs. (4.21)–(4.23) have been carried out as in Ref. 18 by means of 20 points Gauss-Hermite and 10 points Gauss-Laguerre quadrature formulas. Denoting by ξ_p and η_q the corresponding integration points, respectively, the solution of the Schrödinger equation therefore just requires the knowledge of the quantities $\hbar^2/2m^*$, U and W at the mesh points

$$z_p=b_z\xi_p\,,\quad r_q=b_\perp\eta_q{}^{1/2}\,. \tag{4.24}$$

Since we consider only reflection symmetric shapes, only positive values of z_p need in fact to be stored and one is left in this case with a total of 100 mesh points only.

V. RECONSTRUCTION OF DENSITIES IN COORDINATE SPACE

To calculate the average field from the wave functions by means of Eqs. (2.2) it is necessary to evaluate first the nucleon and kinetic energy densities $\rho(r,z)$ and $\tau(r,z)$ and also the functions $\mathrm{div}\vec{J}(r,z)$ and $\nabla^2\rho(r,z)$ at the mesh points (4.24). For the first three quantities this can be readily achieved by means of Eqs. (3.4) and (3.8) from the following expressions for $\Phi_i^{\pm}$, $\nabla_r\Phi_i^{\pm}$, $\nabla_z\Phi_i^{\pm}$ in terms of the expansion coefficients (4.11):

$$\Phi_i^{\pm}(r,z)=\left[\frac{1}{\pi}\beta_z\beta_\perp{}^2e^{-(\xi^2+\eta)}\right]^{1/2}\sum_\alpha\delta_{\Sigma\pm1/2}\delta_{\Lambda\Lambda^{\mp}}C^i_\alpha N_{n_z}N^{\Lambda}_{n_r}\eta^{\Lambda/2}H_{n_z}(\xi)L^{\Lambda}_{n_r}(\eta)\,, \tag{5.1a}$$

$$\nabla_r\Phi_i^{\pm}(r,z)=\left[\frac{1}{\pi}\beta_z\beta_\perp{}^4e^{-(\xi^2+\eta)}\right]^{1/2}\sum_\alpha\delta_{\Sigma\pm1/2}\delta_{\Lambda\Lambda^{\mp}}C^i_\alpha N_{n_z}N^{\Lambda}_{n_r}\eta^{(\Lambda-1)/2}H_{n_z}(\xi)\tilde{L}^{\Lambda}_{n_r}(\eta)\,, \tag{5.1b}$$

$$\nabla_z\Phi_i^{\pm}(r,z)=\left[\frac{1}{\pi}\beta_z{}^3\beta_\perp{}^2e^{-(\xi^2+\eta)}\right]^{1/2}\sum_\alpha\delta_{\Sigma\pm1/2}\delta_{\Lambda\Lambda^{\mp}}C^i_\alpha N_{n_z}N^{\Lambda}_{n_r}\eta^{\Lambda/2}\tilde{H}_{n_z}(\xi)L^{\Lambda}_{n_r}(\eta)\,. \tag{5.1c}$$

The evaluation of the function $\nabla^2\rho(r, z)$ can be carried out in a similar way by means of the relation

$$\begin{aligned}\nabla^2\rho(r, z) &= 2\tau(r, z) + 2\sum_i \Phi_i^* \nabla^2 \Phi_i \\ &= 2\tau(r, z) + 4\sum_{i>0} \{\Phi_i^+(r, z)[\nabla^2 - (\Lambda^-)^2/r^2]\Phi_i^+(r, z) + \Phi_i^-(r, z)[\nabla^2 - (\Lambda^+)^2/r^2]\Phi_i^-(r, z)\}.\end{aligned} \tag{5.2}$$

In Eq. (5.2) the notation $i>0$ means that the summation has to run over positive values of Ω_i only. Here also this simplification occurs because of time-reversal invariance. Finally the quantities $\nabla^2\Phi_i^\pm$ can be obtained immediately from the Schrödinger equation satisfied by the basis states. The result is

$$\begin{aligned}[\nabla^2 - (\Lambda^\mp)^2/r^2]\Phi_i^\pm(r, z) = &\left[\frac{1}{\pi}\beta_z\beta_\perp{}^2 e^{-(\xi^2+\eta)}\right]^{1/2} \sum_\alpha \delta_{\Sigma\pm 1/2}\delta_{\Lambda\Lambda^\mp} C_\alpha^i \\ &\times N_{n_z} N_{n_r}^\Lambda [\beta_z{}^2\xi^2 + \beta_\perp{}^2\eta - 2\beta_z{}^2(n_z+\tfrac{1}{2}) - 2\beta_\perp{}^2(2n_r + |\Lambda| + 1)]\eta^{\Lambda/2} H_{n_z}(\xi) L_{n_r}^\Lambda(\eta).\end{aligned} \tag{5.3}$$

In numerical applications it is most convenient to use as an intermediate step the density matrix in the oscillator basis

$$\rho_{\alpha\beta} = 2\sum_{i>0} n_i C_\beta^{i*} C_\alpha^i, \tag{5.4}$$

where the occupation number n_i is one for occupied states, and zero otherwise. In terms of the $\rho_{\alpha\beta}$'s, the various quantities involved in the definition of the one-body potential are

$$\rho(r, z) = \frac{1}{\pi}\beta_z\beta_\perp{}^2 \exp(-\xi^2-\eta)\sum_{\alpha\beta}\rho_{\alpha\beta}\delta_{\Sigma\Sigma'} N_{n_z} N_{n_z'} N_{n_r}^\Lambda N_{n_r'}^{\Lambda'} \eta^\Lambda H_{n_z}(\xi) H_{n_z'}(\xi) L_{n_r}^\Lambda(\eta) L_{n_r'}^{\Lambda'}(\eta), \tag{5.5a}$$

$$\begin{aligned}\tau(r, z) = &\frac{1}{\pi}\beta_z\beta_\perp{}^2 \exp(-\xi^2-\eta)\sum_{\alpha\beta}\rho_{\alpha\beta}\delta_{\Sigma\Sigma'} N_{n_z} N_{n_z'} N_{n_r}^\Lambda N_{n_r'}^{\Lambda'} \eta^{\Lambda-1} \\ &\times\{\eta\beta_z{}^2 \tilde{H}_{n_z}(\xi)\tilde{H}_{n_z'}(\xi) L_{n_r}^\Lambda(\eta) L_{n_r'}^{\Lambda'}(\eta) + \beta_\perp{}^2 H_{n_z}(\xi) H_{n_z'}(\xi)[\tilde{L}_{n_r}^\Lambda(\eta)\tilde{L}_{n_r'}^{\Lambda'}(\eta) + \Lambda\Lambda' L_{n_r}^\Lambda(\eta) L_{n_r'}^{\Lambda'}(\eta)]\},\end{aligned} \tag{5.5b}$$

$$\begin{aligned}\nabla^2\rho(r, z) = &2\tau(r, z) + \frac{2}{\pi}\beta_z\beta_\perp{}^2 \exp(-\xi^2-\eta)\sum_{\alpha\beta}\rho_{\alpha\beta}\delta_{\Sigma\Sigma'} N_{n_z} N_{n_z'} N_{n_r}^\Lambda N_{n_r'}^{\Lambda'} \eta^\Lambda \\ &\times[\beta_z{}^2\xi^2 + \beta_\perp{}^2\eta - 2\beta_z{}^2(n_z+\tfrac{1}{2}) - 2\beta_\perp{}^2(2n_r + |\Lambda| + 1)] H_{n_z}(\xi) H_{n_z'}(\xi) L_{n_r}^\Lambda(\eta) L_{n_r'}^{\Lambda'}(\eta),\end{aligned} \tag{5.5c}$$

$$\begin{aligned}\mathrm{div}\vec{J}(r, z) = &\frac{2}{\pi}\beta_z{}^2\beta_\perp{}^3 \exp(-\xi^2-\eta)\sum_{\alpha\beta}\rho_{\alpha\beta}\eta^{(\Lambda+\Lambda'-1)/2} N_{n_z} N_{n_z'} N_{n_r}^\Lambda N_{n_r'}^{\Lambda'} \\ &\times\{(\Sigma-\Sigma')H_{n_z}(\xi)\tilde{H}_{n_z'}(\xi)\tilde{L}_{n_r}^\Lambda(\eta) L_{n_r'}^{\Lambda'}(\eta) - |\Sigma-\Sigma'|\Lambda H_{n_z}(\xi)\tilde{H}_{n_z'}(\xi) L_{n_r}^\Lambda(\eta) L_{n_r'}^{\Lambda'}(\eta) \\ &+ 2\delta_{\Sigma\Sigma'}(\beta_\perp/\beta_z)\Lambda\Sigma H_{n_z}(\xi) H_{n_z'}(\xi) L_{n_r}^\Lambda(\eta)\tilde{L}_{n_r'}^{\Lambda'}(\eta)\eta^{-1/2}\}.\end{aligned} \tag{5.5d}$$

VI. COULOMB POTENTIAL

Constructing the average field at the mesh points (4.24) from the densities via Eqs. (2.2) is a trivial step. One difficulty, however, arises in the calculation of the Coulomb field (2.3). The reason is that integrating over the azimuthal angle φ, Eq. (2.3) reduces to

$$\begin{aligned}V_C(r', z') = &\int_0^{+\infty} r\,dr \int_{-\infty}^{+\infty} dz \frac{4e^2\rho_p(r, z)}{[(z-z')^2 + (r+r')^2]^{1/2}} \\ &\times K\left(\{4rr'/[(z-z')^2 + (r+r')^2]\}^{1/2}\right),\end{aligned} \tag{6.1}$$

where K denotes the complete elliptic integral of the first kind

$$K(x) = \int_0^{\pi/2} \frac{d\theta}{(1 - x\sin^2\theta)^{1/2}}. \tag{6.2}$$

The integrand in Eq. (6.1) thus has a logarithmic singularity at the point $r=r'$, $z=z'$. Therefore such a formula is not suitable for numerical integration. A way to bypass this difficulty is to use the relation

$$\nabla_{\vec{R}'}{}^2|\vec{R}-\vec{R}'| = 2/|\vec{R}-\vec{R}'|, \tag{6.3}$$

to carry out two integrations by parts in Eq. (2.3), with the result

$$V_C(\vec{R}) = \tfrac{1}{2}e^2 \int |\vec{R}-\vec{R}'|\,\nabla^2\rho_p(\vec{R}')\,d^3R'. \tag{6.4}$$

Since this expression contains $|\vec{R}-\vec{R}'|$ in the numerator it does not lead to singularities. Indeed after integration over the azimuthal angle φ one finds

$$V_C(r', z') = 2e^2 \int_0^{+\infty} r\,dr \int_{-\infty}^{+\infty} dz[(z-z')^2+(r+r')^2]^{1/2} \times E(\{4rr'/[(z-z')^2+(r+r')^2]\}^{1/2}) \times \nabla^2\rho_p(r, z), \quad (6.5)$$

where E denotes the complete elliptic integral of the second kind

$$E(x) = \int_0^{\pi/2} (1 - x\sin^2\theta)^{1/2}\, d\theta . \quad (6.6)$$

This function is continuous over the interval $[0, 1]$. In practice the integrations in Eq. (6.5) have been carried out by means of Gauss-Hermite and Gauss-Laguerre quadrature formulas using the values of $\nabla^2\rho_p$ already constructed at the mesh points (4.24). The evaluation of the elliptic function (6.6) has been made by means of a standard polynomial-approximation formula.[21]

VII. PAIRING CORRELATIONS

Pairing correlations are known to affect nuclear deformations in the rare-earth region in such a way that they have to be included before making any comparison with experimental data. Also, for heavy nuclei, the density of single-particle states becomes so high that changes in the set of occupied states occur frequently between two successive iterations, therefore slowing down considerably the convergence of the iteration procedure. For these reasons it is necessary to introduce pairing effects at this point. This should be in principle achieved by carrying out complete Hartree-Fock-Bogoliubov calculations. However from the very way Skyrme's interaction is constructed[1, 17] there is no *a priori* reason why it should give a correct description of pairing correlations. Also, due to the presence of a three-body force such calculations would be rather complicated. Therefore in the present work we have preferred to introduce a new parameter to describe pairing. For this purpose let us introduce occupation probabilities n_i for the single-particle states i, such that the definitions for the nucleon, kinetic energy, and spin densities become

$$\rho(\vec{R}) = 2\sum_{i>0} n_i |\Phi_i(\vec{R})|^2,$$
$$\tau(\vec{R}) = 2\sum_{i>0} n_i |\vec{\nabla}\Phi_i(\vec{R})|^2, \quad (7.1)$$
$$\vec{J}(\vec{R}) = -2i\sum_{i>0} n_i \Phi_i^*(\vec{R})(\vec{\nabla}\times\vec{\sigma})\Phi_i(\vec{R}) .$$

Only positive values of Ω appear in Eq. (7.1) because time-reversal invariance requires time-reversed orbits to have equal occupation probabilities. Now in usual pairing theory[19] the pairing energy is given by

$$E_P = -G\{\sum_{i>0}[n_i(1-n_i)]^{1/2}\}^2, \quad (7.2)$$

where G is the pairing strength. To include pairing effects it is therefore natural to extend the variational principle by requiring that the functional

$$E(\Phi_i, n_i) = \int H(\rho, \tau, \vec{J})d^3R - G\{\sum_{i>0}[n_i(1-n_i)]^{1/2}\}^2, \quad (7.3)$$

where H denotes the Hamiltonian density associated with Skyrme's interaction [see Eq. (12) of Ref. 2], should be stationary with respect to individual variations of both the single-particle wave functions Φ_i and the occupation probabilities n_i.

Evaluating the binding energy difference

$$\delta E = E(\Phi_i + \delta\Phi_i, n_i + \delta n_i) - E(\Phi_i, n_i) \quad (7.4)$$

as in Appendix C of Ref. 2, one first obtains

$$\delta E = \sum_i \int d^3R\,[2n_i\delta\Phi_i^*(\vec{R}) + \delta n_i\Phi_i^*(\vec{R})]\left\{-\vec{\nabla}\left(\frac{\hbar^2}{2m^*_{q_i}}\vec{\nabla}\Phi_i\right) + [U_{q_i} + \vec{\nabla}W_{q_i}\cdot(-i)(\vec{\nabla}\times\vec{\sigma})]\Phi_i\right\}$$
$$- G\{\sum_{j>0}[n_j(1-n_j)]^{1/2}\}\sum_{i>0}\delta n_i(1-2n_i)[n_i(1-n_i)]^{-1/2}, \quad (7.5)$$

where the functions $\hbar^2/2m^*$, U, and W are given by Eqs. (2.2) provided that the definitions (7.1) for the densities are used. Since particle number conservation requires the additional constraint

$$\sum_i \delta_{q_i q} n_i = N_q , \quad (7.6)$$

where N_q denotes the number of particles of charge q, the stationarity condition will be written as

$$\delta\Big[E-\sum_i e_i\int d^3R\,|\Phi_i(\vec{R})|^2 - \lambda_n\sum_i \delta_{q_i,-1/2}n_i - \lambda_p\sum_i \delta_{q_i,+1/2}n_i\Big]=0\,. \tag{7.7}$$

Setting the coefficient of $\delta\Phi_i^*$ in the left-hand side of Eq. (7.7) to be equal to zero one first obtains

$$-\vec{\nabla}\cdot\left(\frac{\hbar^2}{2m^*_{q_i}}\vec{\nabla}\Phi_i\right)+[U_{q_i}+\vec{\nabla}W_{q_i}\cdot(-i)(\vec{\nabla}\times\vec{\sigma})]\Phi_i=e_i\Phi_i\,, \tag{7.8}$$

which is identical to (2.1). Next, writing the stationarity condition with respect to variations of the occupation probabilities one finds, by means of (7.8), the following set of equations

$$2(e_i-\lambda_{q_i})[n_i(1-n_i)]^{1/2}-\Delta(1-2n_i)=0\,, \tag{7.9}$$

where the quantity Δ in this equation is

$$\Delta=G\sum_{j>0}[n_j(1-n_j)]^{1/2}\,. \tag{7.10}$$

As in usual pairing theory the only solution of the quadratic equation (7.9) capable of fulfilling the constraint (7.6) is given by the BCS equation[19]

$$n_i=\tfrac{1}{2}\left\{1-\frac{e_i-\lambda_{q_i}}{[(e_i-\lambda_{q_i})^2+\Delta^2]^{1/2}}\right\}. \tag{7.11}$$

The chemical potentials λ_n and λ_p are to be determined from Eq. (7.6).

The functional (7.3) therefore provides a variational principle leading to the occupation-probability distribution of usual pairing theory. From this example the natural question arises whether a variational principle can be constructed for any given probability distribution

$$n_i=f\left(\frac{e_i-\lambda}{\Delta}\right). \tag{7.12}$$

To answer this question let us consider as a generalization of Eq. (7.3) the functional defined by

$$E_P=-G[\sum_{i>0}\varphi(n_i)]^2\,, \tag{7.13}$$

where G is a constant which has the dimension of an energy. One can see very easily in this case that Eq. (7.8) remains unchanged whereas the BCS equation (7.11) has to be replaced by

$$e_i-\lambda=\Delta\varphi'(n_i)\,, \tag{7.14}$$

where Δ is now given by

$$\Delta=G\sum_{j>0}\varphi(n_j)\,. \tag{7.15}$$

Therefore if $\varphi(x)$ denotes an indefinite integral of $f^{-1}(x)$, Eq. (7.13) is a solution of our problem. As an example it may be seen that the occupation-probability distribution defined by a Fermi function

$$n_i=\frac{1}{1+\exp(e_i-\lambda/\Delta)} \tag{7.16}$$

is the BCS equation corresponding to the pairing functional

$$E_P=-G\{\sum_{i>0}[n_i\ln n_i+(1-n_i)\ln(1-n_i)]\}^2\,. \tag{7.17}$$

The gap Δ is defined in this case by

$$\Delta=-G\sum_{i>0}\{n_i\ln n_i+(1-n_i)\ln(1-n_i)\}\,. \tag{7.18}$$

Similarly one can work out from the previous procedure a pairing functional corresponding to the Strutinsky smoothing function[22]

$$n_i=\tfrac{1}{2}\left[1+\mathrm{erf}\left(\frac{e_i-\lambda}{\Delta}\right)\right]. \tag{7.19}$$

The solution to the previous problem is not at all unique. For instance all the functionals

$$E_P=F[\sum_{i>0}\varphi(n_i)]\,, \tag{7.20}$$

where F is an arbitrary (differentiable) function, give the same BCS equation (7.14). The only difference is that the gap equation (7.15) has to be replaced by

$$\Delta=-\tfrac{1}{2}F'[\sum_{i>0}\varphi(n_i)]\,. \tag{7.21}$$

Since the only feature of pairing theory we are really interested in for the present calculation is the possibility of having a diffuse Fermi surface, we have used this degree of freedom in order to construct the simplest gap equation, namely a constant gap. The corresponding pairing functional is

$$E_P=-2\Delta\sum_{i>0}[n_i(1-n_i)]^{1/2}\,. \tag{7.22}$$

By construction, the use of either functionals (7.2) or (7.22) is guaranteed to give identical ground-state wave functions, i.e. identical Φ_i's and n_i's, provided the gap Δ in Eq. (7.22) is taken to be the diffuseness (7.10) of the occupation-probability distribution obtained from Eq. (7.2). In particular, both functionals give identical values for the quadrupole moments, radii and density distributions.

In the present work the choice of the constant Δ in Eq. (7.22) has been made according to the empirical formula[23]

$$\Delta\simeq 12\ \mathrm{MeV}\times A^{-1/2}\,. \tag{7.23}$$

A constant value $\Delta = 1$ MeV has been used in all calculations in the rare-earth region. In the case of light-nuclei pairing effects have been neglected.

One shortcoming of the present simplified treatment of pairing correlations is that even though it gives correct wave functions, and therefore at least a correct description of the dominant effects of pairing on deformations, it does not give a correct pairing energy. Indeed, although both functionals (7.2) and (7.22) reach their minima simultaneously, it may be seen from Eq. (7.10) that the functional (7.22) gives twice as much pairing energy as (7.2) at equilibrium. However, for the purpose of comparing calculated binding energies to experimental ones, this difference is not too important since in the rare-earth region, pairing energies are typically of the order of 0.1 MeV per particle, i.e., of the order of truncation effects in this case as will be seen in Sec. VIII.

To solve the system of Eqs. (7.1), (7.6), (7.8), and (7.11) a calculation of the occupation probabilities n_i (7.11) has been included at the end of each iteration of the Hartree-Fock procedure. The equation for the chemical potential (7.6) has been first rewritten, by means of Eq. (7.11) as

$$g(\lambda) \equiv \sum_{i>0} \left\{ 1 - \frac{e_i - \lambda}{[(e_i - \lambda)^2 + \Delta^2]^{1/2}} \right\} = N \qquad (7.24)$$

and its solution has been carried out by the Newton-Raphson iteration method:

$$\lambda_{k+1} = \lambda_k + [N - g(\lambda_k)]/g'(\lambda_k),$$

$$g'(\lambda) = \sum_{i>0} \frac{\Delta^2}{[(e_i - \lambda)^2 + \Delta^2]^{3/2}} .$$

One definite advantage of the present treatment of pairing correlations is that it is free of divergences in the case of a continuum of positive energy states with a level density proportional to $\sqrt{E}$.[19] Indeed it may be checked that, since occupation probabilities n_i behave like Δ^2/e_i^2 as e_i goes to infinity, the integral occurring in this case in the left-hand side of Eq. (7.24) is a convergent one.

VIII. RESULTS

Results presented in this section have been obtained by solving the Hartree-Fock equations (2.1) and (2.2) for the two sets of parameters defined in Table I. We recall that in the case of rare-earth nuclei pairing effects have been included by adding to the Hartree-Fock equations a set of BCS equations with a constant gap $\Delta = 1$ MeV (7.1), (7.11), and (7.24). Unless otherwise specified the oscillator expansion (4.11) occurring in the solution of the deformed Schrödinger equation has been truncated at five major shells ($N_0 = 4$) for light nuclei, and seven major shells ($N_0 = 6$) for rare-earth nuclei. In all calculations the two oscillator parameters have been chosen so as to minimize the total binding energy. For consistency with the calculations already presented in Ref. 2, the Coulomb exchange terms have been neglected and only the direct term in the center-of-mass correction has been included. A discussion of the uncertainties arising from these approximations may be found in Ref. 17. Since center-of-mass corrections decrease with mass number our approximate treatment of these corrections is believed to be adequate in the rare-earth region. As was mentioned in Sec. II, the small contributions from the central force to the one-body spin-orbit potential have also been neglected. Since larger contributions of the same form would also be obtained from the tensor force,[24] it would be meaningless to include these terms without including at the same time a proper description of the tensor force in the Skyrme effective interaction.

Typical computation times on an IBM 360/65, including minimization with respect to both oscillator parameters, are of the order of 20 min for a light nucleus ($N_0 = 4$), 50 min in the rare-earth region ($N_0 = 6$), and 120 min if the basis is truncated at nine major shells only ($N_0 = 8$). Calculations in the actinide region would require a basis including eleven major shells, i.e., a total computation time of the order of four hours for one nucleus on an IBM 360/65. A definite advantage of the present method of solving the deformed Hartree-Fock equations is that no matrix elements of the interaction need to be stored, so that our code may be used without tapes or disks even in the actinide region with $N_0 = 10$. We would also like to point out that the present method of solution is not restricted to a linear density dependence in the effective interaction, so that it could be used as well for the modified delta interaction of Moszkowski[4] which contains a density dependence proportional to $\rho^{2/3}$.

A. Binding Energies

Calculated charge radii, binding energies, and charge quadrupole moments for some light and rare-earth nuclei are given in Table II. In the case of light nuclei these results are also compared in Fig. 1 with experimental data and with the results obtained by Zofka and Ripka[8] using a slight modification of Negele's interaction.[5] It may be seen from this figure that calculated binding energies agree remarkably well with the experimental ones. The fit is somewhat better than

that of Zofka and Ripka for both interactions, and better for force I than force II. However, one should keep in mind that projecting out a 0^+ ground state out of the deformed Slater determinant would lower the energy of the system. The gain in energy in the case of neon-20 was estimated by Zofka and Ripka to be of the order of 0.2 MeV per particle. Even though this number should presumably be reduced in the case of interaction I, since it gives smaller deformations than Negele's force, neon-20 would be overbound after angular momentum projection in the case of interaction I, while for interaction II a value very close to the observed one should be obtained. In the rare-earth region calculated binding energies per particle also agree quite well with experimental data, predicted values being generally too small by 0.3 MeV (0.6 MeV) for interaction I (II). Here again however, these values would be increased by angular momentum projection, and also, as will be seen in subsection F, by increasing the size of the oscillator basis.

The variation of binding energies per particle as a function of mass number in light nuclei may be seen from Fig. 1 to be very similar for interaction II and for the Negele interaction used by Zofka and Ripka. The reason for this similarity is that, by means of the density matrix expansion presented in Ref. 17, a set of parameters for the Skyrme force may be derived from Negele's interaction. This set turns out to be very close to our parameter set II. In particular it gives rise to almost identical nonlocality effects in the average nuclear field. This is related to the great similarity in the effective masses $m^*/m \simeq 0.6$ obtained for both forces in nuclear matter.

Projected α-cluster configurations for light nuclei have been calculated by Friedrich, Hüsken, and Weiguny[25] for interactions I and II. These turn out to be significantly less bound than Hartree-

TABLE II. Binding energies per particle, root-mean-square charge radii, and charge quadrupole moments calculated with interactions I and II. Equilibrium values for the volume oscillator parameter β_0 and for the deformation parameter q have also been indicated. Experimental values for light nuclei have been extracted from Zofka and Ripka (Ref. 8). For such nuclei experimental quadrupole moments are those obtained from Coulomb excitation measurements, which do not determine the sign of this quantity.

	β_0 (fm^{-1})	q	E/A (MeV)	r_c (fm)	Q (barns)
			^{12}C		
I	0.700	1.00	8.11	2.44	0.00
II	0.659	0.718	6.84	2.64	−0.14
Exp	···	···	7.68	2.40 ± 0.03	0.205 ± 0.015
			^{20}Ne		
I	0.661	1.28	8.00	2.88	0.34
II	0.621	1.39	7.48	3.02	0.46
Exp	···	···	8.03	···	0.54 ± 0.03
			^{24}Mg		
I	0.651	1.30	8.40	3.01	0.50
II	0.610	1.30	7.68	3.15	0.60
Exp	···	···	8.26	3.01	0.67 ± 0.04
			^{28}Si		
I	0.652	0.860	8.67	3.05	−0.26
II	0.607	0.710	7.86	3.26	−0.60
Exp	···	···	8.45	3.09 ± 0.03	0.55 ± 0.02
			^{32}S		
I	0.636	1.20	8.60	3.17	0.28
II	0.599	1.28	7.90	3.32	0.52
Exp	···	···	8.49	3.24 ± 0.02	0.47 ± 0.03
			^{36}Ar		
I	0.618	0.821	8.50	3.30	−0.36
II	0.588	0.831	8.10	3.42	−0.48
Exp	···	···	8.52	···	0.54 ± 0.06
			^{152}Sm		
I	0.474	1.35	8.04	5.06	5.30
II	0.449	1.20	7.67	5.15	3.20
Exp	···	···	8.24	5.09[a]	5.78 ± 0.10[a] 5.90[b]
			^{160}Gd		
I	0.465	1.40	7.94	5.16	6.76
II	0.439	1.38	7.55	5.28	7.02
Exp	···	···	8.18	···	7.56[b]
			^{170}Er		
I	0.458	1.36	7.82	5.25	7.00
II	0.431	1.34	7.44	5.38	7.44
Exp	···	···	8.11	5.26[a]	7.75 ± 0.10[a] 7.40[b]

[a] Reference 28.
[b] Reference 35.

Fock solutions, the difference being of the order of 1 MeV per particle. For instance the binding energy of carbon-12 calculated by the previous authors using force I is 6.38 MeV per particle before projection and 6.64 MeV per particle after projection. In neon-20 the corresponding value using the same interaction is 7.26 MeV per particle before angular momentum projection. On the other hand, in the case of the interaction B1 of Brink and Boeker,[26] very similar binding energies are found for α-cluster configurations and Hartree-Fock solutions, α configurations being energetically favored for nuclei lighter than magnesium-24.[27] This difference arises because the Brink and Boeker force has no two-body spin-orbit term, a much stronger P-wave repulsion, and also because the Skyrme force is a simple parametrization of the effective interaction which is valid for low relative momenta only. In particular it becomes infinitely repulsive for high momenta, whereas the finite-range B1 interaction goes to zero in this case. Therefore α-cluster configurations are much less favored in the case of the Skyrme force since they contain relatively high excitations when expended in terms of shell-model wave functions.

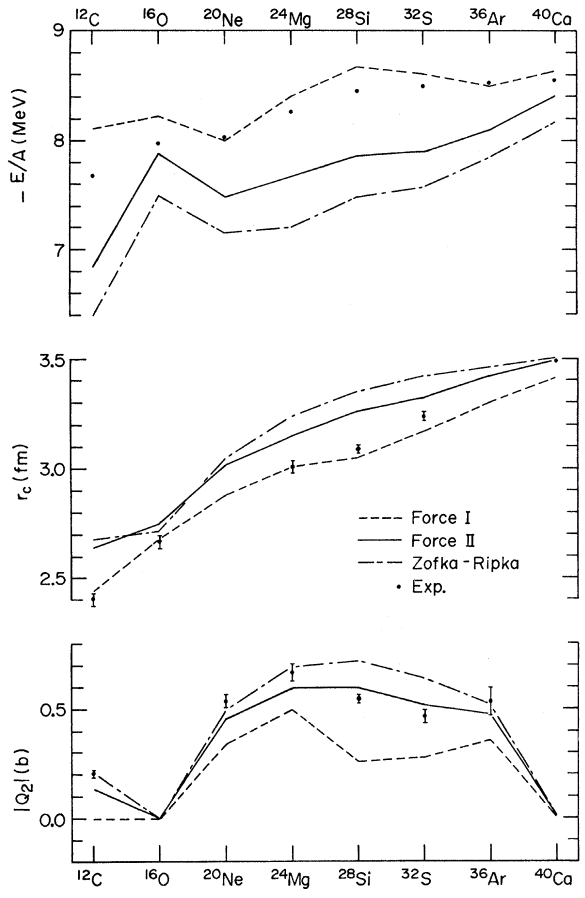

FIG. 1. Comparison of binding energies, charge radii, and absolute values of the charge quadrupole moments obtained in light nuclei from interactions I and II, with the results of Zofka and Ripka (Ref. 8) and with experimental data. Experimental data points are taken from Ref. 8.

In light nuclei, deformed Hartree-Fock calculations using similar density-dependent forces have been made by Lassey and Volkov,[14] and by Krieger and Moszkowski.[15] Binding energies calculated by these authors also agree rather well with the observed ones, and are in fact very close to those obtained from interaction II. In contrast, calculations made with density independent forces[9-13] always give a lack of binding of the order of 2 MeV per particle.

B. Radii

The charge radii of light nuclei, which have been corrected for the finite size of the proton, may be seen from Fig. 1 and Table II to be in close agreement with the experimental ones for both interaction I and II. In fact for interaction I the fit is excellent up to sulfur-32, while a somewhat too small value is obtained in calcium-40. For both forces the agreement is somewhat better than those obtained by Zofka and Ripka,[8] Lassey and Volkov,[14] and Krieger and Moszkowski.[15] Radii calculated by Lassey and Volkov are systematically too small, while Zofka and Ripka find too large values for deformed nuclei, and Krieger and Moszkowski too small radii for the spherical ones. Here again a great similarity may be observed in the variation of radii as a function of mass number for interaction II and for the Negele interaction used by Zofka and Ripka.[8]

Accurate measurements from muonic x-ray data are available in the rare-earth region.[28] Calculated values may be seen from Table II to be in excellent agreement with these measurements for interaction I, and in good agreement for interaction II. As will be seen in subsection F this agreement is unaffected if a larger oscillator basis is used.

C. Charge Quadrupole Moments

Quadrupole moments of the proton distributions do not need to be corrected for the finite extent of the proton in order to obtain the quadrupole moments of charge. Indeed, since the charge distribution ρ_c is constructed by folding the proton density ρ_p and the proton form factor f_p, one has

$$Q_c = \int d^3R d^3R' (2z^2 - x^2 - y^2) \rho_p(\vec{R}') f_p(|\vec{R} - \vec{R}'|) . \tag{8.1}$$

Rewriting the first term in the previous integral as

$$2z^2 - x^2 - y^2 = 2(z - z')^2 + 4(z - z')z' + 2z'^2 - (x - x')^2 - 2(x - x')x' - x'^2 - (y - y')^2 - 2(y - y')y' - y'^2,$$

Eq. (8.1) becomes

$$Q_c = Z\int d^3R(2z^2 - x^2 - y^2)f_p(\vec{R}) + Q_p,$$

where Z is the charge of the nucleus. Since the form factor of the proton is spherically symmetric, this last equation implies that $Q_c = Q_p$.

Whereas very similar results were obtained from interactions I and II for binding energies and radii, Fig. 1 shows that the situation is rather different for deformations in light nuclei. Indeed, while charge quadrupole moments obtained from force II agree very well with those extracted from Coulomb excitation measurements, much smaller values are obtained from interaction I. In particular, carbon-12 turns out to be spherical in this last case.

As will be shown in subsection E, the two-body spin-orbit interaction reduces nuclear deformations significantly in light nuclei. However, even though force I has a stronger spin-orbit component than force II (see Table I), this difference does not explain satisfactorily the difference in quadrupole moments. Indeed, if the two-body spin-orbit strength of interaction I is reduced to 80 MeV fm^5, the quadrupole moment of neon-20 increases to 0.41 b, which is still smaller than the value obtained from force II with a spin-orbit strength of 105 MeV fm^5.

Surface effects also reduce nuclear deformations and for this reason, we calculated for both forces the surface energy coefficient W_s defined as the second coefficient in the expansion

$$E/A = a_0 + W_s A^{-1/3} + \cdots . \tag{8.2}$$

For this purpose, spherical Hartree-Fock calculations of $N = Z$ nuclei, without Coulomb and spin-orbit interactions, were carried out for $A = 125$ and $A = 1000$ using the filling parameter approximation.[29] The value of a_0 being known to be -16 MeV for both forces,[2] a value of W_s may be extracted from Eq. (8.2) as a function of A. The result given in Table III shows that the values of W_s are already converged for $A = 125$. Actually these values are slightly larger than those calculated by Lassey,[30] and by Ravenhall, Bennett, and Pethick[31] using a semi-infinite slab model. We attribute this difference to the persistence of shell fluctuations in our densities, even for $A = 1000$. Table III also shows that the value of the surface energy coefficient W_s is larger for interaction II than for interaction I. Thus, the difference in nuclear deformations cannot be attributed to a difference in surface properties.

TABLE III. Binding energies per particle E/A (MeV), obtained from spherical Hartree-Fock calculations without spin-orbit and Coulomb interaction for $A = 125$ and $A = 1000$. Values of the surface energy coefficient W_s (MeV) are extracted from Eq. (8.2).

	Force I		Force II	
A	125	1000	125	1000
E/A	−11.85	−13.93	−11.60	−13.72
W_s	20.76	20.68	21.99	22.05

The previous difference seems to be rather connected with the difference in the effective masses in nuclear matter, which was already mentioned in Sec. II as being the most significant difference between forces I and II. Indeed for a small change in the single-particle wave functions, the change δE in the total energy of the system is given by[32]

$$\delta E = \int d^3R\left(\frac{\hbar^2}{2m^*(\vec{R})}\,\delta\tau(\vec{R}) + U(\vec{R})\delta\rho(\vec{R})\right). \tag{8.3}$$

In this equation $\delta\tau$ and $\delta\rho$ denote the changes in the kinetic energy and nucleon densities, respectively, and $\hbar^2/2m^*$ and $U(\vec{R})$ are defined by Eq. (2.2). Approximating the effective mass m^* by its nuclear-matter value, the previous equation becomes

$$\delta E = \frac{m}{m^*}\delta T + \int d^3R\, U(\vec{R})\delta\rho(\vec{R}), \tag{8.4}$$

where δT denotes the change in the kinetic energy of the system. Now, as will be shown in subsection E, the kinetic energy of a nucleus decreases significantly as it becomes deformed. Therefore a smaller value of the effective mass will provide a bigger gain in energy when deforming the nucleus, i.e., larger equilibrium deformations.

The previous remark also explains the similarity between the deformations obtained from interaction II and from the Negele force used by Zofka and Ripka,[8] since both forces have almost identical effective masses in nuclear matter. In fact, this similarity would be even greater if a two-body spin-orbit term had been included in the calculations of Zofka and Ripka. Including this term allows a better fit to quadrupole moments of nuclei heavier than magnesium-24. It also favors the oblate solution of silicon-28 and the prolate solution of sulfur-32, which agrees with the results of Tuerpe, Bassichis, and Kerman.[7] The absence

of a two-body spin-orbit force in the calculations of Lassey and Volkov,[14] and of Krieger and Moszkowski[15] also explains why our results for interaction II are somewhat better than theirs.

It is interesting to note that interaction II was also found in Ref. 2 to give the best fit to the observed energies of 1s-proton levels. As was already mentioned in Sec. II, the position of these levels is related also to the value of the effective mass m^*/m from Eq. (2.1).

As was discussed by Zofka and Ripka, all experimental methods to determine quadrupole moments of the intrinsic states assume the validity of the rotational model,[16] which is not well established for light nuclei. For this reason it would be much more satisfactory for such nuclei to compare the measured $B(E2)$ values to those calculated from angular momentum states projected out of the Hartree-Fock ground state. On the other hand, in the rare-earth region, it may be shown[33,34] that, due to the large expectation values $\langle J^2 \rangle$ obtained for the square of the angular momentum, quadrupole moments for the first excited 2^+ states may be accurately approximated by rotational-model values. There is indeed very little doubt about the validity of this model in the rare-earth region and it is certainly legitimate to use it in this case to extract quadrupole moments for the intrinsic states.

From Table II the charge quadrupole moments calculated for gadolinium-160 and erbium-170 may be seen to agree quite well for both interactions I and II with the experimental values obtained from Coulomb excitation measurements[35] and muonic x-ray data.[28] In contrast in samarium-152 there exists a discrepancy in the case of interaction II, the calculated value being too small by about 40%. The origin of this discrepancy may be understood from spherical Hartree-Fock calculations in the neighborhood of samarium. Indeed such calculations show that interaction I gives a neutron closed shell at $N=90$ with a 0.24-MeV gap and a proton closed shell at $Z=64$ with a 2-MeV gap. For interaction II, the neutron shell closure occurs at $N=92$ with a 1.5-MeV gap, while the proton shell closes at $Z=64$ with a 1.6-MeV gap. Therefore, in the case of interaction II, samarium-152 is near double closure with two rather important gaps. From the results obtained in lead-208 in Ref. 2, it seems that the tendency of interaction II to overemphasize shell effects is systematic. A possible way of correcting this defect would be to allow the strength t_1 of the velocity-dependent term in the Skyme force to depend linearly on the density. In this case Eq. (2.2b) would contain an additional quadratic term in density. This term should make it possible to have simultaneously an effective mass of the order of 0.6 inside the nucleus (which seems necessary to fit 1s-proton levels[2]), and 1.2 in the surface region (which seems appropriate to reproduce the observed level density of lead-208[36]).

As in light nuclei, deformations in the rare-earth region are smaller for interaction I than for interaction II (if one excludes the case of samarium-152 which was discussed above). The difference, however, is much less than in light nuclei. Indeed, we will see in subsection E that the mechanism for nuclear deformations is somewhat different between the two regions. Whereas the two-body spin-orbit force inhibits deformations in light nuclei, it will be shown to favor deformations in the rare-earth region. Also the Coulomb interaction is more effective in heavier nuclei and tends to level off differences in the effective masses between the two interactions. Another possibility is the symmetry effect. All the light nuclei we discussed above are $N=Z$ systems and are therefore insensitive to the parameter x_0 in the Skyrme interaction.[37] On the other hand rare-earth nuclei have a significant neutron excess, so that deformations for such nuclei may, *a priori*, exhibit a dependence on x_0. To investigate the importance of this effect we decreased the value of x_0 in interaction II from 0.34 to 0.23, since this brings the value of the symmetry energy coefficient a_τ in nuclear matter from 34.1 MeV to the interaction I value of 29.3 MeV.[38] In this case the quadrupole moment of gadolinium-160 decreases from 7.02 b to a value of 6.82 b, which is closer to the result obtained from force I (6.76 b).

D. Density Distributions

A convenient representation of deformed density distributions is through the Legendre expansion coefficients defined by

$$\rho(r, \theta) = \rho_0(r) + \rho_2(r) P_2(\cos\theta) + \rho_4(r) P_4(\cos\theta) + \cdots . \tag{8.5}$$

These may be evaluated in a simple way from the values of the densities at the mesh points (4.24) as is described in Appendix B.

The first few coefficients in this expansion are shown in Fig. 2 for the charge distributions of neon-20 and samarium-152 calculated with interaction I. For both nuclei similar qualitative features are obtained: $\rho_2(r)$ and $\rho_4(r)$ are nonnegligible only in the surface region, so that the density is nearly constant in the nuclear interior, as should be expected from the saturation properties of the Skyrme force. This may also be seen on Fig. 3 where we have plotted the variation of the charge density of samarium-152 in the case of

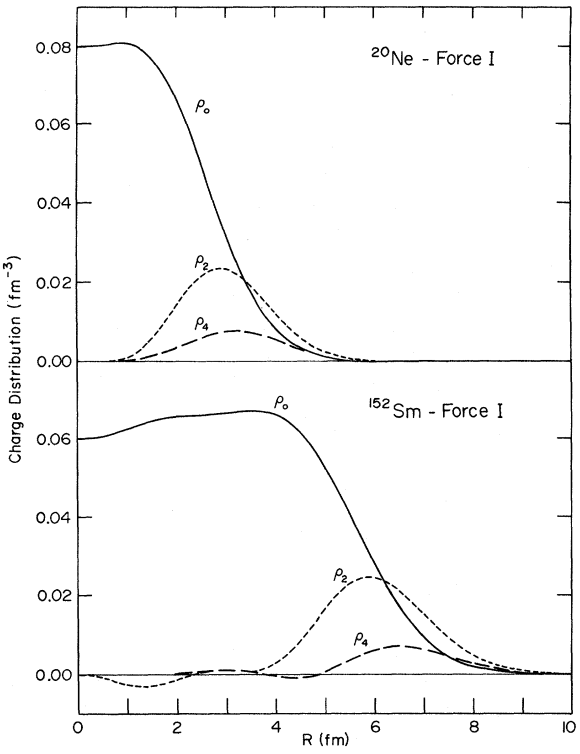

FIG. 2. Legendre expansion coefficients for the charge distributions of neon-20 and samarium-152 calculated with interaction I.

interaction I along the symmetry axis ($r=0$) perpendicular to the symmetry axis ($z=0$) and along the direction $z=r$, i.e., $\theta=45°$ in Eq. (8.5). A slight depression may be observed at the center of the nucleus, which is due to the fact that in a spherical shell model the $3s_{1/2}$ proton orbit would be empty in samarium. While in phenomenological distributions[28,39] the surface thickness of $\rho(r, \theta)$ for a given θ is assumed to be independent of θ, a small change in this quantity is obtained when θ changes: Whereas the maximum slope is 0.0571 fm^{-4} for $z=0$, it is 0.0537 fm^{-4} for $z=r$ and 0.0588 fm^{-4} for $r=0$. This change tends to produce parallel equidensity lines in the surface region, which agrees with the conclusions of Damgaard *et al.*[18]

The first two coefficients of the Legendre expansions for the charge distributions calculated in erbium-170 from interactions I and II are compared in Fig. 4 with those obtained from muonic x-ray measurements.[28] For both forces a rather good agreement is obtained except for the surface thicknesses which tend to be somewhat larger for the Hartree-Fock densities. This quantity, however, does not seem to be very accurately determined experimentally, and slightly different values are in fact obtained from electron scattering data. For instance in the case of samarium-152, the value of the parameter t in the phenomenological

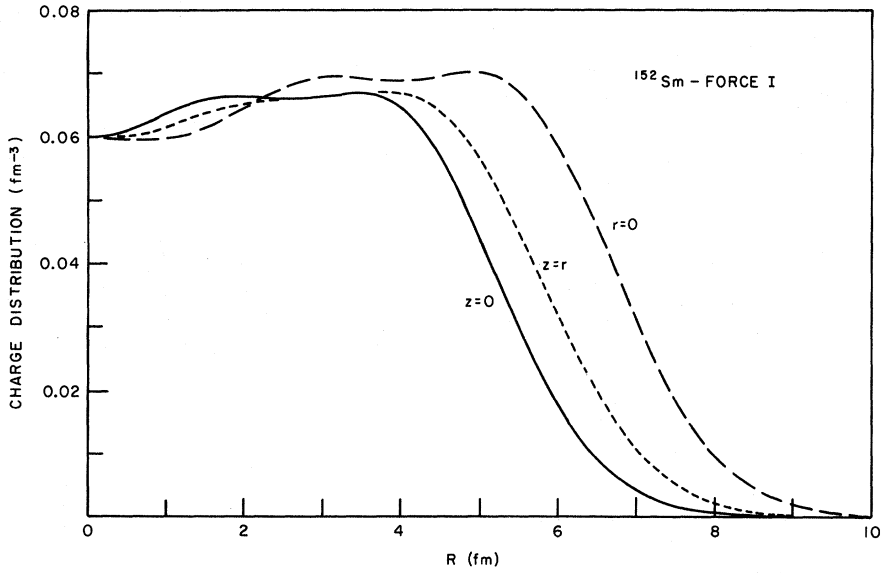

FIG. 3. Sections of the charge distribution $\rho(R, \theta)$, calculated in samarium-152 with interaction I for $\theta=0$ ($r=0$), $\theta=45°$ ($z=r$), and $\theta=90°$ ($z=0$).

distribution

$$\rho(r,\theta)=\bar{\rho}\left[1+\exp\left(\frac{r-R(\theta)}{t}\right)\right]^{-1},$$

$$R(\theta)=c(1+\beta_2 Y_{20}(\theta)+\cdots),$$

is found to be 0.538 ± 0.012 fm from muonic x rays, while it is 0.581 ± 0.040 fm from recent electron scattering experiments.[39] This last value is in better agreement with our results.

E. Comparison of Spherical and Deformed Solutions

Since our calculations include a two-body spin-orbit interaction, the Hartree-Fock equations have solutions with spherical symmetry in the case of carbon-12, silicon-28, and sulfur-32. Such solutions also exist for rare-earth nuclei because pairing effects have been taken into account in this region. A detailed comparison of the deformed solutions with the spherical ones is very useful as far as it indicates what terms in the two-body interaction contribute most to the binding energy difference. It may therefore provide a basis for understanding the mechanism of nuclear deformations. For consistency, spherical solutions have been calculated in as oscillator basis even though calculations in configuration space would be possible in this case.

Such a comparison is made in Table IV in the case of sulfur-32 (force I), samarium-152 (force I) and silicon-28 (force II). A systematic decrease may be observed in Coulomb and kinetic energies as the nucleus becomes deformed. It is rather small for Coulomb energies but turns out to be quite significant for kinetic energies, so that the change in this quantity appears to play a dominant role in nuclear deformations. An important effect is also obtained from the two-body spin-orbit interaction, whose contributions to the total binding energy exhibits large fluctuations as a function deformation. This force may be seen from Table IV to favor strongly spherical solutions in light nuclei, but to favor deformed solutions in the rare-earth region. It is interesting to note that a similar conclusion would also be obtained in the framework of the Nilsson model.[16] Indeed, in this model, the effect of a stronger spin-orbit coupling in the rare-earth region is to bring down levels from higher shells into the neighborhood of the Fermi level, which produces larger deformations. On the other hand this effect does not occur in light nuclei because of the absence of low-lying unoccupied orbits with high degeneracy.

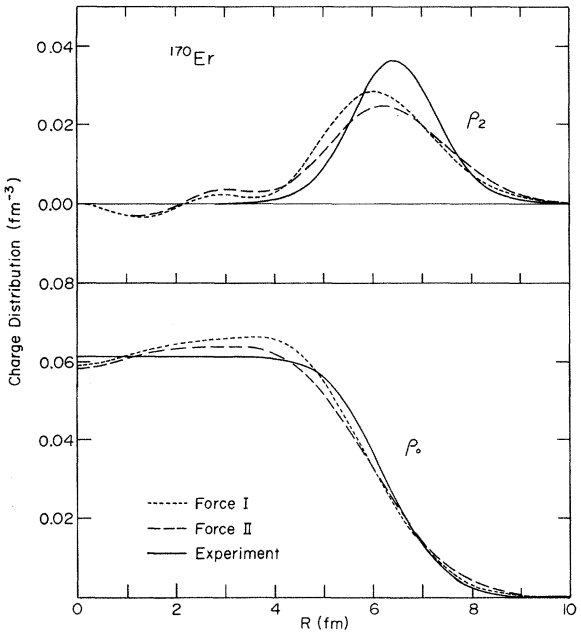

FIG. 4. Legendre expansion coefficients for the charge distributions of erbium-170 obtained from interaction I, II, and muonic x-ray measurement in Ref. 28.

TABLE IV. Comparison of kinetic, Coulomb, spin-orbit, pairing, and binding energies (in MeV) of spherical and deformed solutions for sulfur-32 (force I), samarium-152 (force I), and silicon-28 (force II). Values of charge radii r_c (fm), volume oscillator parameters β_0 (fm^{-1}), and deformation parameters q are also indicated.

	^{32}S (I)		^{152}Sm (I)		^{28}Si (II)	
	sph.	def.	sph.	def.	sph.	def.
E_{kin}	582.27	577.89	2903.87	2893.20	468.19	451.22
E_{Coul}	57.05	56.88	524.16	522.64	43.54	42.90
E_{so}	−43.81	−38.53	−67.26	−77.39	−33.14	−20.57
E_{pair}	0	0	−35.95	−28.93	0	0
E	−274.68	−275.15	−1215.65	−1221.98	−215.04	−220.08
r_c	3.153	3.166	5.003	5.059	3.165	3.259
β_0	0.638	0.636	0.478	0.474	0.605	0.607
q	1.00	1.20	1.00	1.35	1.00	0.71

TABLE V. Variation of the volume oscillator parameter β_0 (fm^{-1}), deformation parameter q, binding energy per particle E/A (MeV), charge radius r_c (fm), and charge quadrupole moment Q (b), as a function of the size N_0 of the oscillator basis defined by Eq. (4.14).

	^{20}Ne		^{152}Sm	
N_0	4	6	6	8
β_0	0.661	0.663	0.474	0.523
q	1.28	1.34	1.35	1.37
E/A	8.004	8.038	8.039	8.312
r_c	2.878	2.876	5.059	5.048
Q	0.344	0.347	5.30	5.81

Pairing correlations may be seen from Table IV to inhibit nuclear deformation, as was already noted in the early stage of pairing theory.[40] An explanation for this effect is that the pairing interaction tends to smear out orbits near the Fermi level, therefore producing a state with higher spatial symmetry. Table IV also gives the value of the volume oscillator parameter β_0 at equilibrium. This parameter may be seen to change only very slightly as the nucleus becomes deformed, which may be related to the underlying assumption of constant volume in the Nilsson model.[16]

F. Truncation Effects

In this section, some of the previous results are compared to the results obtained in a larger oscillator basis including two more major shells, i.e., $N_0 = 6$ for light nuclei and $N_0 = 8$ for rare-earth nuclei. This comparison will be made here in the case of interaction I only, but very similar results would be obtained for interaction II. It may be seen from Table V that a very satisfactory convergence is obtained in neon-20 with an oscillator basis containing five major shells only. Indeed, including two more shells in the oscillator expansion increases the binding energy per particle by less than 50 keV, while a negligible change is obtained for the root-mean-square charge radius. A larger variation is found to occur for the charge quadrupole moment, in agreement with the results of Tuerpe, Bassichis, and Kerman.[7] The change, however, is still less than 1% in this case.

For samarium-152, truncation effects may be seen from Table V to be more important, but still small enough, however, to make a comparison with experimental data meaningful. When increasing the size of the oscillator basis from $N_0 = 6$ to $N_0 = 8$, a gain of approximately 300 keV is obtained for the binding energy per particle, while the root-mean-square charge radius decreases by 0.2%. At the same time, the charge quadrupole moment increases by 10%, which brings the calculated value in closer agreement with the observed one.

Equilibrium values for the volume oscillator parameter β_0 always increase with the size of the basis N_0. This is because our choice of basis vectors implies nearly pure oscillator configurations for orbits close to the Fermi level in the case of a small basis. On the other hand, a larger basis allows high- and low-lying orbits to have similar admixtures. The optimum value of the volume oscillator parameter is therefore essentially determined by the radius of the nucleus in the case of a large basis, while only the radius of the last orbit seems to matter in the case of a small basis.

The convergence of the charge distribution of samarium-152 is investigated in Fig. 5, where we have plotted the first two coefficients $\rho_0(r)$ and

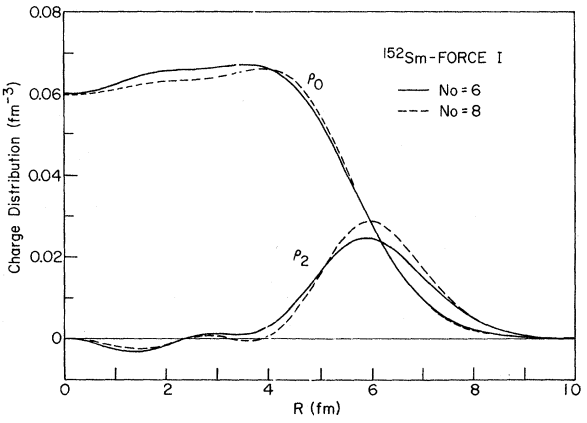

FIG. 5. Variation of the Legendre expansion coefficients for the charge distribution of samarium-152, calculated with interaction I, as a function of the size parameter N_0 of the oscillator basis.

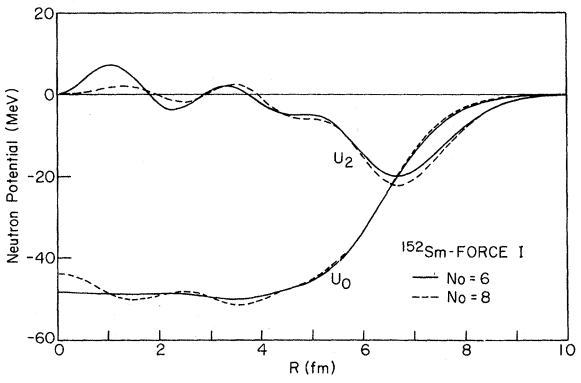

FIG. 6. Variation of the Legendre expansion coefficients for the neutron potential of samarium-152, calculated with interaction I, as a function of the size parameter N_0 of the oscillator basis.

$\rho_2(r)$ in the Legendre expansion (8.5), for two different sizes of the oscillator basis, $N_0=6$ and $N_0=8$. While only slight differences occur for the coefficient ρ_0, larger deviations are obtained for the coefficient ρ_2, which is related to the fact that truncation effects are more important for quadrupole moments than for radii. Even larger variations would be obtained for the coefficient $\rho_4(r)$. In the case of light nuclei a much better convergence of the oscillator expansion is obtained and graphs of $\rho_0(r)$ or $\rho_2(r)$ corresponding to $N_0=4$ and $N_0=6$ would hardly be distinguishable on the scale of Fig. 5.

The variation of the neutron potential (2.2a) as a function of N_0 is shown in Fig. 6 in the case of samarium-152. From this figure, truncation effects may be seen to be similar for the average potential and for the density.

IX. CONCLUSION

A method for solving the deformed Hartree-Fock equations in the case of the Skyrme interaction has been presented, which is applicable to the region of heavy deformed nuclei. Calculations have been made using two different sets of parameters for some light and rare-earth nuclei, and it has been demonstrated that the Skyrme force can provide a very good description of binding energies, radii, and quadrupole moments of these nuclei.

Several applications of the techniques described in the present paper are possible. In particular, the previous method for solving the deformed Hartree-Fock equations may be easily extended to the case of realistic reaction matrices, provided use is made of the density matrix expansion presented in Ref. 17. It would therefore be possible to calculate deformations of heavy nuclei in terms of a realistic nucleon-nucleon force. Also by adding an external field to the Hartree-Fock Hamiltonian, as described in Ref. 41, it would be possible to evaluate the energy of a heavy nucleus as a function of its shape, which represents a first step towards a microscopic description of fission isomers and fission barriers, and also provides a very convenient basis for understanding the validity of Strutinsky's prescription.[22]

ACKNOWLEDGMENTS

It is a great pleasure to express my deep appreciation to D. M. Brink for many discussions concerning the feasibility of making Hartree-Fock calculations in deformed nuclei with the Skyrme interaction and also for his help in deriving the formulas in Secs. III, IV, and V. I am also most grateful to M. Véneroni, A. K. Kerman, and G. E. Brown for numerous illuminating discussions and suggestions throughout the course of this work. My thanks are also due J. Heisenberg for fruitful discussions concerning density distributions, and J. P. Vary for a critical reading of the manuscript.

APPENDIX A. NUMBER OF MATRIX ELEMENTS

Due to time-reversal invariance only basis vectors $\{n_r, n_z, \Lambda, \Sigma\}$ such that $\Lambda+\Sigma=\Omega>0$ need to be considered. Assuming the number N_0 characterizing the size of the oscillator basis in Eq. (4.14) to be even, the number of such states is

$$N=\sum_{n_r=0}^{N_0/2}\sum_{n_z=0}^{N_0-2n_r}\left(1+2\sum_{\Lambda=1}^{N_0-2n_r-n_z}1\right)$$

$$=\tfrac{1}{6}(N_0+1)(N_0+2)(N_0+3)\,. \tag{A1}$$

Since $\Omega=\Lambda+\Sigma$ and the parity $\pi=(-1)^{n_z+\Lambda}$ are good quantum numbers, the Hamiltonian matrix (4.13) is block diagonal. Denoting by $D(\Omega,\pi)$ the dimension of the block (Ω,π) one has

$$D(\Omega,\pi)=\sum_{\Lambda=\Omega-1/2}^{\Omega+1/2}\left(\sum_{n_z=0}^{N_0-\Lambda}\tfrac{1}{2}[1+(-1)^{n_z+\Lambda+\pi}]\sum_{n_r=0}^{(N_0-n_z-\Lambda)/2}1\right).$$

The summations in the previous equations may be carried out in a straightforward way. The result is

$$D(\Omega,\pi)=\tfrac{1}{4}(N_0-\Omega+2+\tfrac{1}{2}P)(N_0-\Omega+2+\pi-\tfrac{1}{2}P)\,,$$

where

$$P=(-1)^{\Omega-1/2}\,. \tag{A2}$$

The total number of nonvanishing matrix elements is given by

$$F(N_0)=D^2(N_0+\tfrac{1}{2},\ \pi=+1)+\sum_{\Omega=1/2}^{N_0-1/2}\sum_{\pi}D^2(\Omega,\pi)\,. \tag{A3}$$

Inserting Eq. (A2) into Eq. (A3), the previous expression may be transformed into the following form

$$F(N_0)=\left(\frac{N_0+2}{2}\right)^4+2\sum_{n=1}^{N_0/2}[n^4+n^2(n+1)^2]\,.$$

The sums of powers in the previous equation may be performed by means of standard formulas,[21] with the result

$$F(N_0)=\tfrac{1}{40}(N_0+2)(N_0^2+2N_0+2)(N_0^2+6N_0+10)\,. \tag{A4}$$

From this relation one finds $F(6)=820$, $F(8)=2501$, $F(10)=6222$, $F(12)=13\,447\ldots$.

APPENDIX B. CALCULATION OF DENSITY DISTRIBUTIONS

The present method of solving the Hartree-Fock equations uses only values of the densities at the mesh points (4.24). These are sufficient, however, to reconstruct values of the densities at an arbitrary point (r, z) without returning to the expansion coefficients (4.11), which would be numerically quite a lengthy procedure. Indeed the nucleon densities in the truncated basis may be written as

$$\rho(r,z)=\exp(-\beta_z^2 z^2-\beta_\perp^2 r^2)P(r^2,z^2)\,, \tag{B1}$$

where P is a polynomial of degree N_0 in both r^2 and z^2. Expressing this polynomial in terms of Hermite and Laguerre polynomials

$$P(r^2,z^2)=\sum_{k=0}^{N_0}\sum_{l=0}^{N_0} N_{2k}H_{2k}(\beta_z z)N_l^0 L_l^0(\beta_\perp^2 r^2)A_{kl}\,,$$

the expansion coefficients A_{kl} are found to be

$$A_{kl}=\pi\beta_z\beta_\perp^2\int_0^{+\infty}d\eta\int_{-\infty}^{+\infty}d\xi\,\rho(b_z\xi,b_\perp\eta)\times N_{2k}H_{2k}(\xi)N_l^0L_l^0(\eta)\,. \tag{B2}$$

Since P in Eq. (B1) is a polynomial, Hermite- and Laguerre-Gauss integration formulas are exact when applied to the previous integral provided the number of integration points is greater than N_0. The result is

$$A_{kl}=2\sum_{ij}\pi_i\omega_j\rho(b_z\xi_i,b_\perp\eta_j^{1/2})\times N_{2k}H_{2k}(\xi_i)N_l^0L_l^0(\eta_j)\,,$$

where π_i, ω_j and ξ_i, n_j denote the weights and abscissas of the Hermite- and Laguerre-Gauss quadrature formulas, respectively.

The calculation of the Legendre expansion coefficients in Eq. (8.5) may be easily carried out by using the orthogonality properties of the Legendre polynomials,[21] with the result

$$\rho_k(r)=(2k+1)\int_0^{\pi/2}\rho(r\cos\theta,r\sin\theta)P_k(\cos\theta)\sin\theta\,d\theta\,.$$

In the case of the charge density

$$\rho_c(\vec{R})=\int f_p(|\vec{R}-\vec{R}'|)\rho_p(\vec{R}')d^3R'\,, \tag{B3}$$

the evaluation of the Legendre expansion coefficients is also straightforward. Denoting these coefficients by $\bar{\rho}_k(r)$ and inserting into Eq. (B3) the multipole expansion for the form factor of the proton

$$f_p(|\vec{R}-\vec{R}'|)=\sum_{k\mu}\frac{4\pi}{2k+1}v_k(R,R')Y_{k\mu}^*(\Omega')Y_{k\mu}(\Omega)\,,$$

one obtains

$$\bar{\rho}_k(r)=\frac{4\pi}{2k+1}\int_0^{+\infty}\rho_k(r')v_k(r,r')r'^2dr'\,.$$

In terms of the Legendre expansion coefficients the quadrupole and the octupole moments are given, respectively, by

$$Q_2=\frac{8\pi}{5}\int_0^{+\infty}\rho_2(r)r^4dr\,,\qquad Q_4=\frac{8\pi}{9}\int_0^{+\infty}\rho_4(r)r^6dr\,.$$

---

*Work supported in part through funds provided by the Atomic Energy Commission under Contract AT(11-1)-3069.

[1]T. H. R. Skyrme, Phil. Mag. 1, 1043 (1956); Nucl. Phys. 9, 615 (1959).
[2]D. Vautherin and D. M. Brink, Phys. Rev. C 5, 626 (1972).
[3]H. S. Köhler, Nucl. Phys. A170, 88 (1971).
[4]S. A. Moszkowski, Phys. Rev. C 2, 402 (1970); J. W. Ehlers and S. A. Moszkowski, *ibid.* 6, 217 (1972).
[5]J. W. Negele, Phys. Rev. C 1, 1260 (1970); similar work has been carried out recently by X. Campi and D. W. L. Sprung, Nucl. Phys. A194, 401 (1972).
[6]J. Nemeth and D. Vautherin, Phys. Letters 32B, 561 (1970).
[7]D. R. Tuerpe, W. H. Bassichis, and A. K. Kerman, Nucl. Phys. A142, 49 (1970).
[8]J. Zofka and G. Ripka, Nucl. Phys. A168, 65 (1971).
[9]P. U. Sauer, A. Faessler, H. H. Wolter, and M. M. Stingl, Nucl. Phys. A125, 257 (1969).
[10]S. J. Krieger, Phys. Rev. C 1, 76 (1970).
[11]R. Muthukrishnan, Nucl. Phys. A93, 417 (1967).
[12]M. Bouten, M. C. Bouten, H. Depuydt, and L. Schotmans, Phys. Letters 33B, 457 (1970).
[13]M. Manning, Ph.D. thesis, McMaster University, 1967 (unpublished).
[14]K. R. Lassey and A. B. Volkov, Phys. Letters 36B, 4 (1971).
[15]S. J. Krieger and S. A. Moszkowski, Phys. Rev. C 5, 1990 (1972).
[16]S. G. Nilsson, Kgl. Danske Videnskab. Selskab, Mat.-Fys. Medd. 29, No. 16 (1955).
[17]J. W. Negele and D. Vautherin, Phys. Rev. C 5, 1472 (1972).
[18]J. Damgaard, H. C. Pauli, V. V. Paskhevich, and V. M. Strutinsky, Nucl. Phys. A135, 432 (1969).
[19]See, for instance, A. M. Lane, *Nuclear Theory* (Benjamin, New York, 1964).
[20]F. Dickmann, Z. Physik 203, 141 (1967); E. O. Fiset, J. R. Nix, and E. M. Bolsterli, Los Alamos Report No. LA-4735-MS, 1971 (unpublished).
[21]See, for instance, M. Abramowitz and I. A. Stegun, *Handbook of Mathematical Functions* (Dover, New York, 1968).

[22]M. Brack, J. Damgaard, A. S. Jensen, H. C. Pauli, V. M. Strutinsky, and C. Y. Wong, Rev. Mod. Phys. 44, 320 (1972).
[23]A. Bohr and B. Mottelson, *Nuclear Structure* (Benjamin, New York, 1969), Vol. 1, p. 169.
[24]See Sec. 4 of Ref. 17.
[25]H. Friedrich, H. Hüsken, and A. Weiguny, Phys. Letters 38B, 199 (1972).
[26]D. M. Brink and E. Boeker, Nucl. Phys. A91, 1 (1967).
[27]D. M. Brink, H. Friedrich, A. Weiguny, and C. W. Wong, Phys. Letters 33B, 143 (1970).
[28]D. Hitlin *et al.*, Phys. Rev. C 1, 1184 (1970).
[29]W. H. Bassichis and A. K. Kerman, Phys. Rev. C 2, 1768 (1970).
[30]K. R. Lassey Nucl. Phys. A192, 177 (1972).
[31]D. G. Ravenhall, C. D. Bennet, and C. J. Pethick, Phys. Rev. Letters 28, 978 (1972).
[32]See Eq. (C2) of Ref. 2. For simplicity we have assumed and equal number of neutrons and protons. We have also omitted the contribution from the two-body spin-orbit force, since its effect was already discussed.
[33]F. M. H. Villars, in *Many-Body Description of Nuclear Structure and Reactions, International School of Physics "Enrico Fermi," Course XXXVI,* edited by C. Bloch (Academic, New York, 1966).
[34]G. Ripka, *Advances in Nuclear Physics* (Plenum, New York, 1968), Vol. 1.
[35]R. Graetzer and E. M. Bernstein, Phys. Rev. 129, 1772 (1963).
[36]G. E. Brown, J. H. Gunn, and P. Gould, Nucl. Phys. 46, 598 (1963); G. F. Bertsch and T. T. S. Kuo, Nucl. Phys. A112, 204 (1968).
[37]For a nucleus with $N=Z$, the parameter x_0 cancels out identically in the Hartree-Fock equations provided neutron and proton wave functions are assumed to be identical. See Eqs. (23) and (24) of Ref. 2.
[38]See Table II of Ref. 2.
[39]W. Bertozzi *et al.*, Phys. Rev. Letters 28, 1711 (1972).
[40]S. T. Belyeav, Kgl. Danske Videnskab. Selskab.,Mat.-Fys. Medd. 31, No. 11 (1959).
[41]W. H. Bassichis, A. K. Kerman, C. F. Tsang, D. R. Tuerpe, and L. Wilets, University of California Radiation Laboratory Report No. UCRL-73044 (to be published).

PHYSICAL REVIEW C VOLUME 7, NUMBER 1 JANUARY 1973

Inelastic Proton Scattering Angular Distributions*

J. H. Degnan, B. L. Cohen, G. R. Rao, K. C. Chan, and L. Shabason
University of Pittsburgh, Nuclear Physics Laboratory, Pittsburgh, Pennsylvania 15213
(Received 16 August 1972)

A new technique for determining inelastic angular distributions, which greatly alleviates the background problem, is described. Application of the technique to (p,p') reactions with targets ^{122}Sn, ^{119}Sn, and ^{112}Sn is discussed and the results are compared with results using a more conventional technique. The results are that the differential cross section is forward peaked at all energies for (p,p') reactions with targets ^{119}Sn and ^{122}Sn, while it is approximately isotropic with the target ^{112}Sn at higher excitation energies of the residual nucleus. The ^{112}Sn result is expected from the previously established predominance of ordinary compound-nucleus processes in that reaction. For ^{119}Sn and ^{122}Sn in which it was previously presumed that isospin-conserving reactions via $T_>$ states dominate the low-energy portion of the proton spectrum, the results indicate a sizable contribution of direct reactions or of pre-equilibrium reactions with very few collisions.

I. INTRODUCTION

Knowledge of the inelastic scattering angular distribution gives information on the reaction mechanism. An isotropic distribution or one symmetric about 90° is characteristic of a compound-nucleus (CN) reaction mechansim, while a distribution which is forward peaked or highly correlated with the incident beam direction is characteristic of a direct reaction (DR) mechanism.[1]

Measurement of the inelastic scattering angular distribution is complicated by background problems. This background is presumably due to: (1) slit scattering of the incident beam (which introduces low-energy components to the beam, which are strongly elastically scattered by the target); (2) slit scattering of elastically scattered particles (and higher-energy inelastically scattered particles) by the detector slit; and (3) reactions in the detector (in which the detected particle does not cause a pulse with the full pulse height for its energy). These problems can be minimized (but not eliminated) by excellent beam tuning, by placing the detector slit between a large area ΔE detector and a smaller area E detector, and using a tight particle selection window. Since the background is roughly proportional to the elastic scattering cross section,[2] it increases rapidly as the